Antarctica
Thermosphere-Ionosphere Fe/Fe^+ (TIFe) Layers
Lidar Observations & Numerical Modeling

Xinzhao Chu and Zhibin Yu
University of Colorado Boulder

Discovery Hut

Gratefully Acknowledge
Art Richmond, Chester S. Gardner, Cao Chen, Weichun Fong, Zhonghua Xu, J. M. C. Plane, W. Feng, J. D. Carrillo-Sanchez, J. Forbes, R. Bishop, J. Zhao, S. Solomon, H.-L. Liu, D. R. Weimer, D. J. Knipp, B. Foster, T. Fuller-Rowell, R. Robinson, S. L. Vadas, A. Burns, X. Pi, L. M. Kilcommons, J. S. Friedman, W. Huang, X. Lu, Z. Wang, J. A. Smith, J. P. Thayer, and V. Papitashvili, et al.

Science Highlight @ CEDAR 2018

McMurdo Lidar Observations since Dec 2010

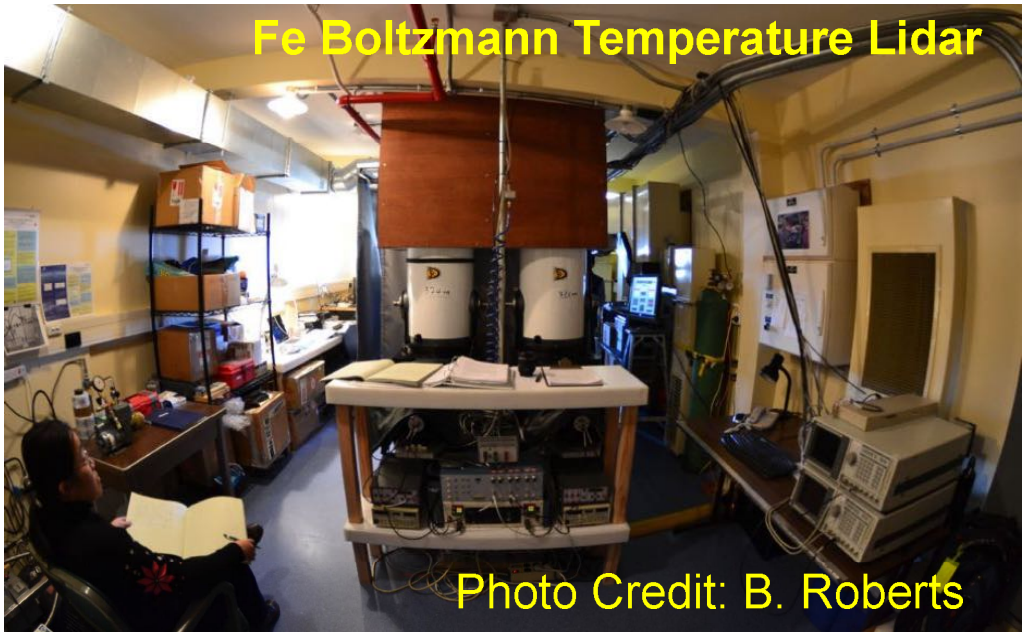

McMurdo lidar projects supported by NSF grants OPP-0839091, 1246405, and 1443726

Highlights of McMurdo Lidar Discoveries

McMurdo lidar observations filled a critical data gap between the South Pole and Antarctic Circle

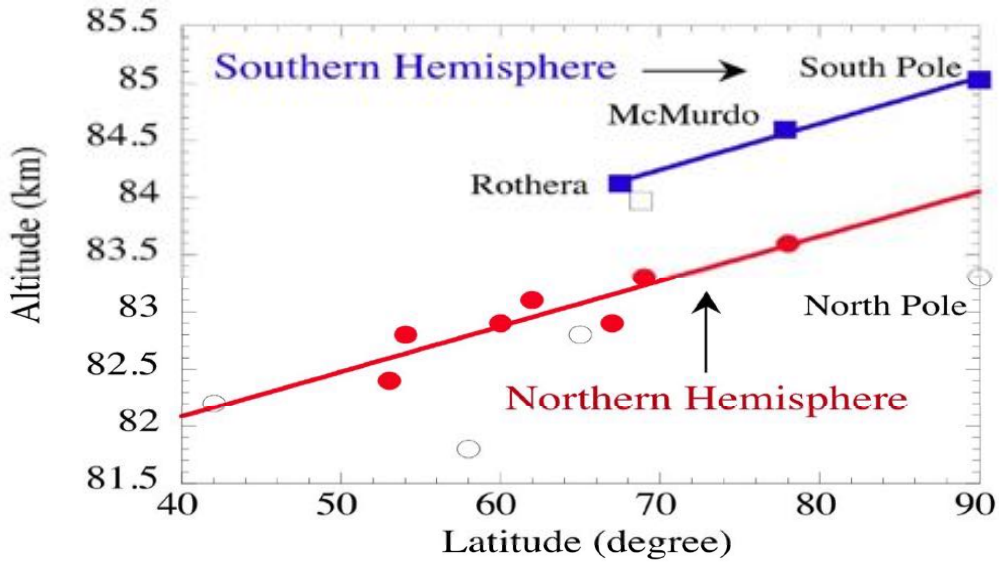

Polar Mesospheric Clouds

Hemispheric Difference and Latitudinal Dependence in PMC Altitudes
[Chu et al., GRL, 2011a]

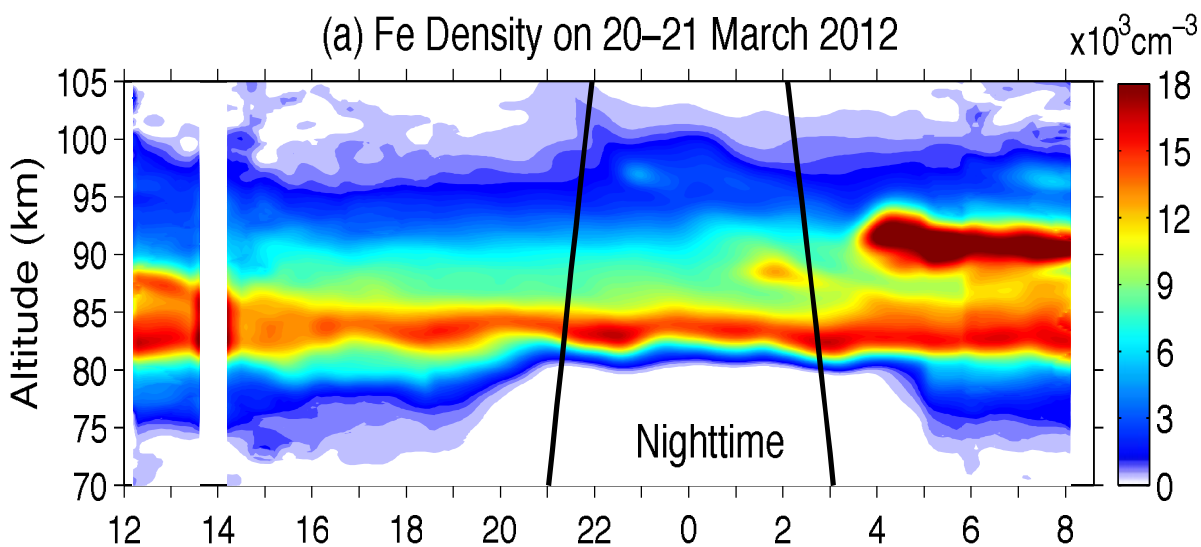

Solar effects on mesospheric Fe layers
[Yu et al., JGR, 2012]

Discovery of the solar effect on mesospheric Fe layer bottomside

Discovery of Persistent Gravity Waves with Periods of 3–10 h and λ_z of 20–30 km

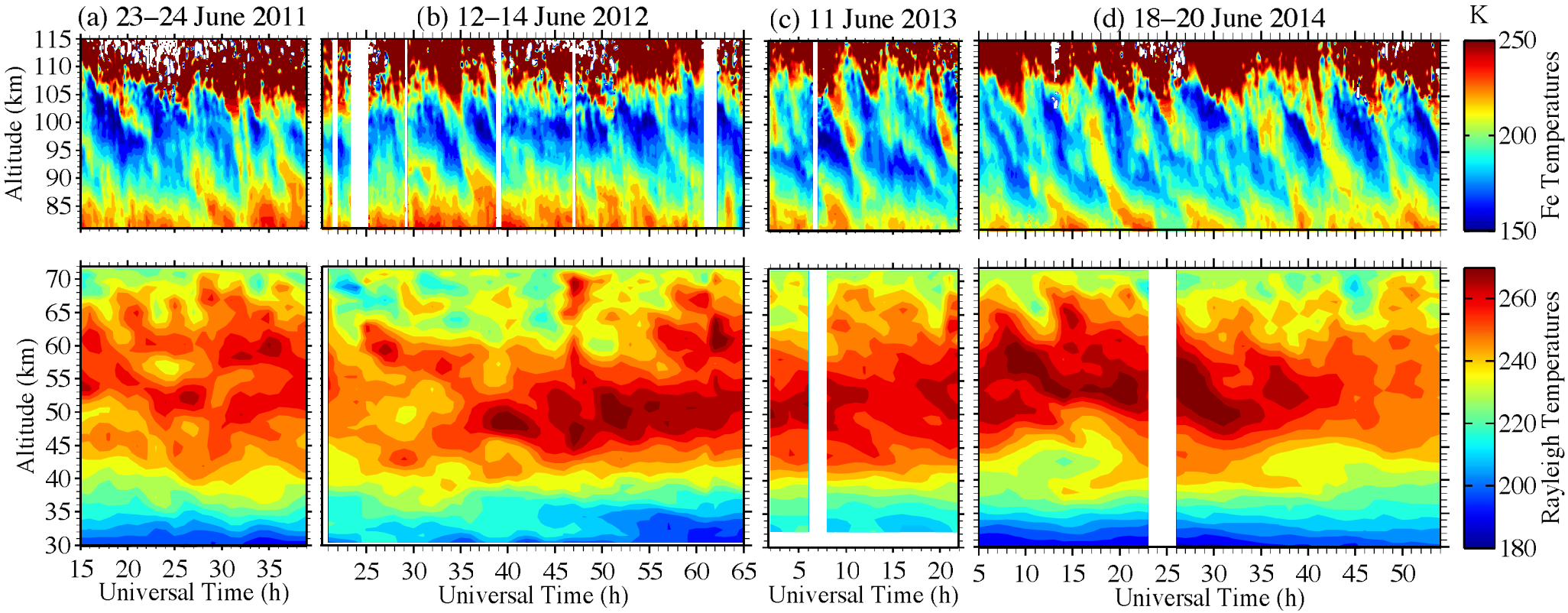

[Chen et al., JGR-Space Physics, 2016]

Persistent, large-amplitudes, dominant (±20–30 K)

As a group, these waves are perpetual

Occurring on every lidar run

McMurdo lidar observations challenge current GCMs?

Lidar Discovery Inspired Modelers to Search for the Wave Sources → Secondary Gravity Wave Generation (Vadas and Becker)

High-Resolution KMCM

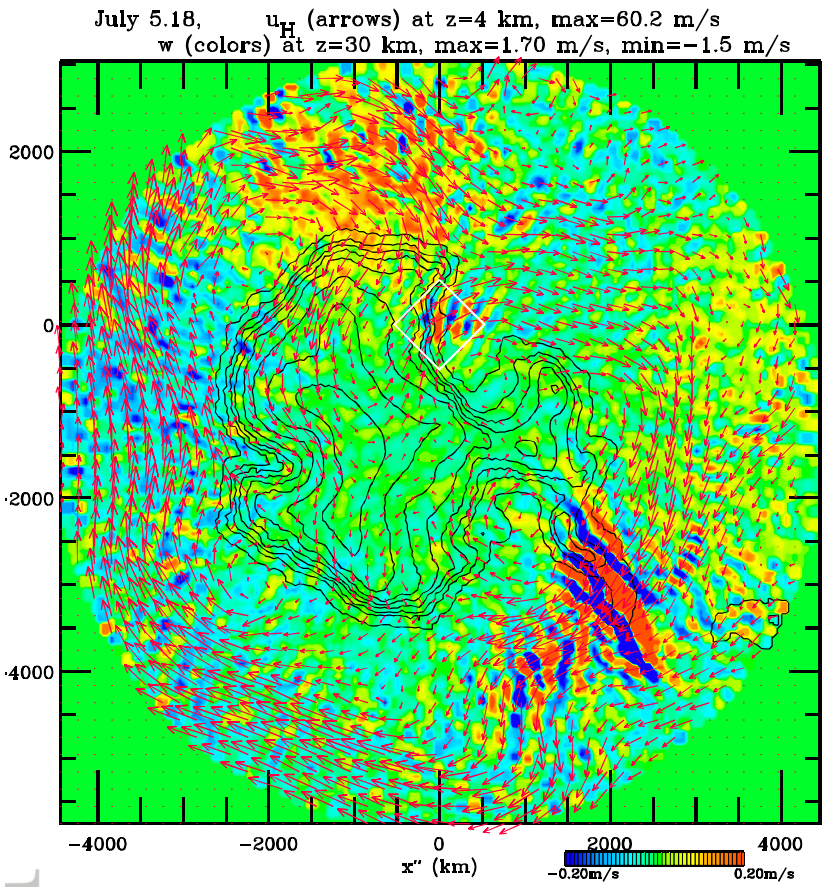

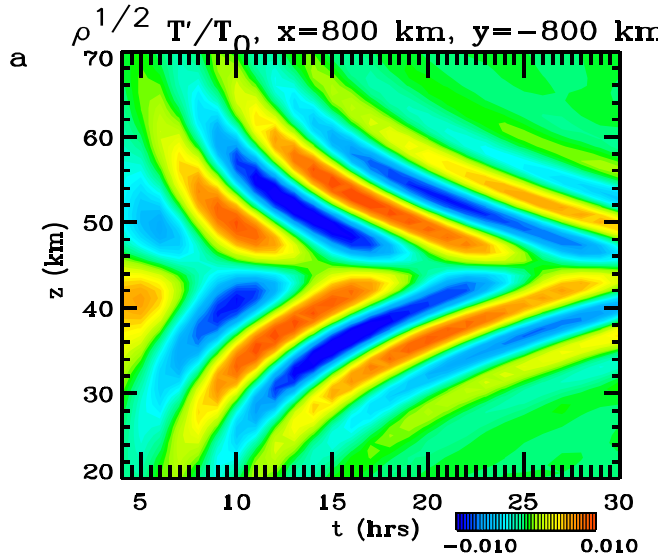

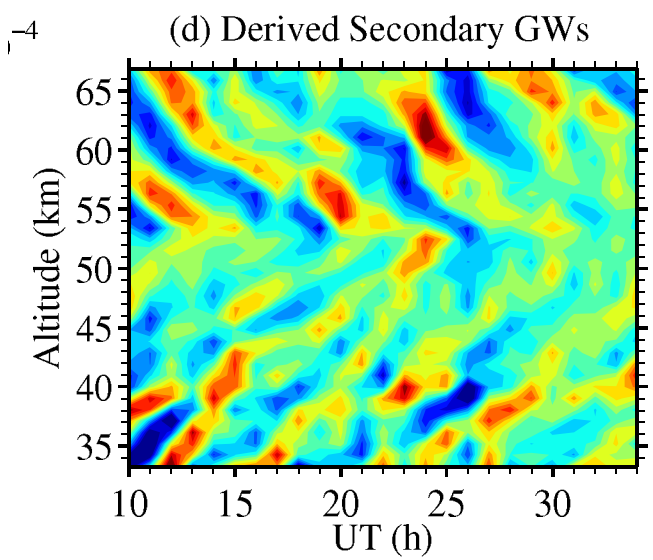

Vadas Theoretical Prediction

Lidar-obs Fishbone Structure

[Becker and Vadas, 2018; Vadas and Becker, 2018; Vadas et al., 2018]

Multi-Year Lidar Observations Enabled Statistical Characterization of Gravity Waves in the Stratosphere

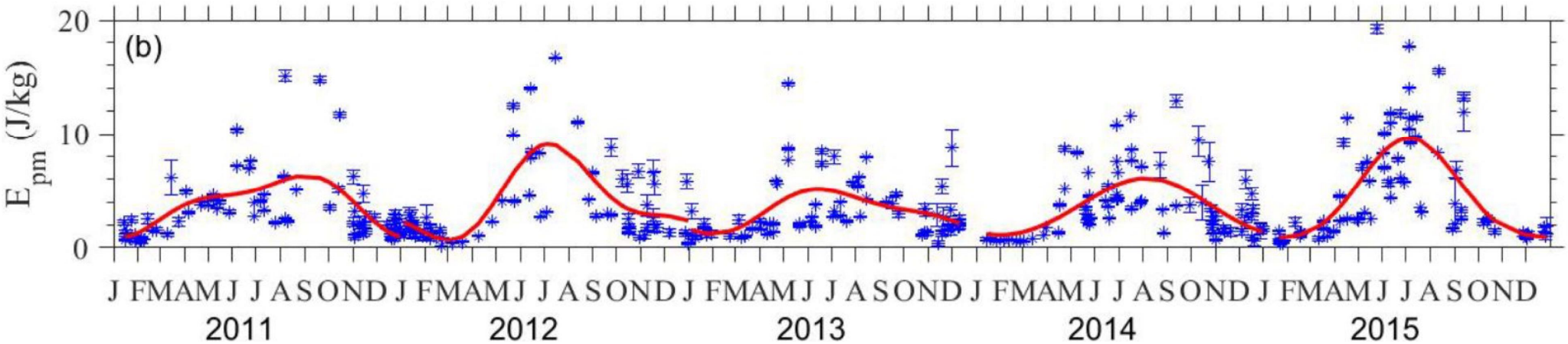

[Chu et al., JGR, 2018]

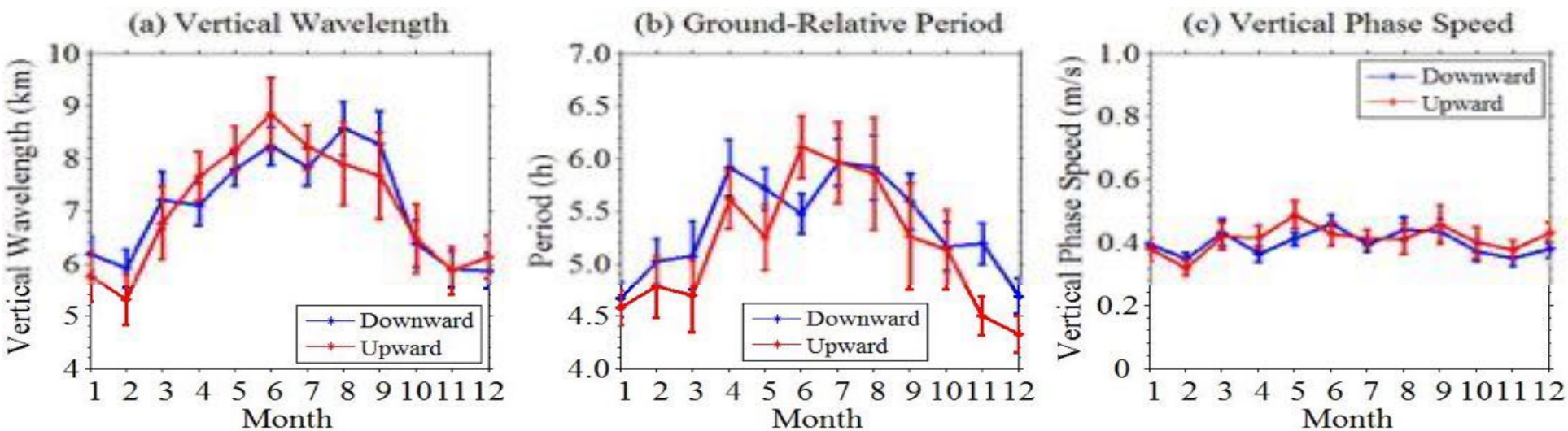

[Zhao et al., JGR, 2017]

McMurdo lidar obs. are in the 8th year – Hope to cover a solar cycle

Multi-Day Lidar Observations Enabled Studies of Planetary Waves (30-110 km)

Lidar PWs (30-110 km)

Satellite PWs (MLS)

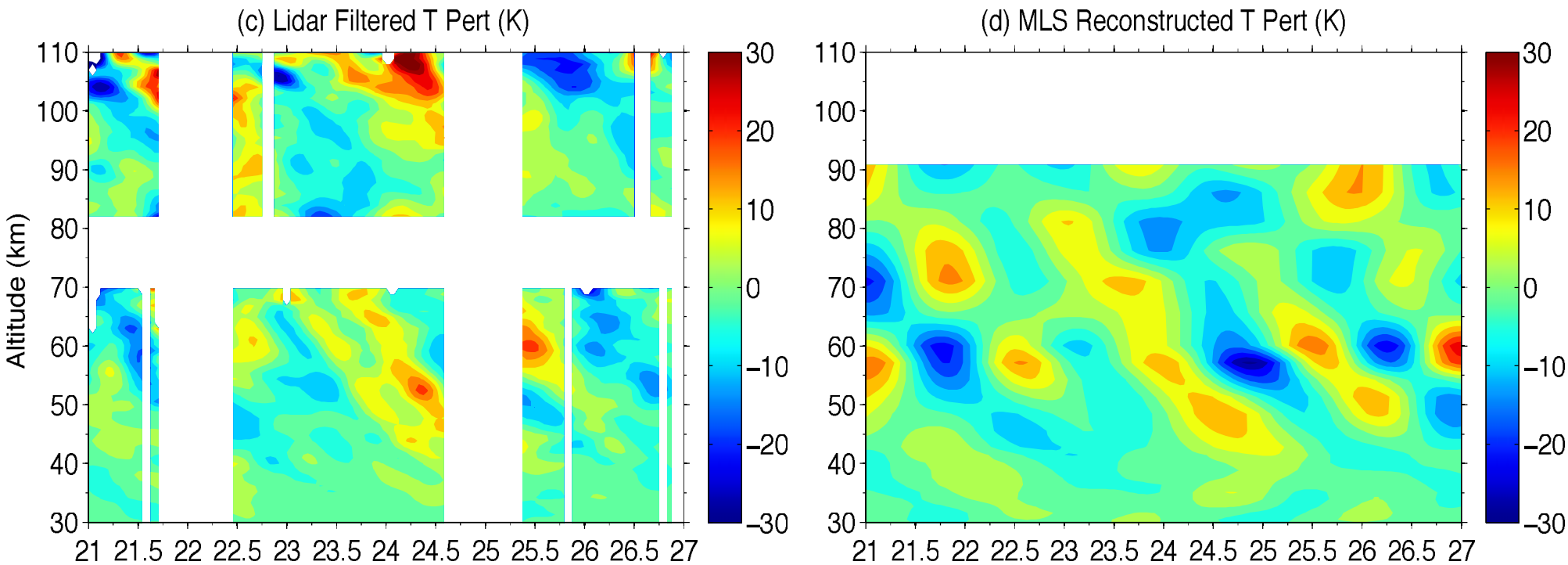

[Lu et al., GRL, 2017; JGR, 2015]

The multi-day McMurdo lidar observations combining satellite data (MLS) enabled better characterization and quantification of baroclinic planetary waves generated by polar vortex in a very deep vertical range, especially providing information above 100 km.

Aurora Effect on the Fast Amplitude Growth of Temperature Tides in the Lower Thermosphere

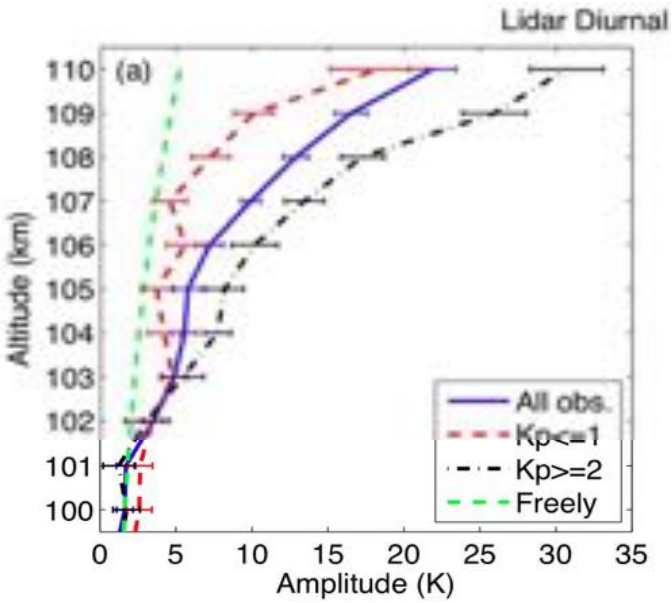

(a) Diurnal Tide

Hall-ion-drag induced adiabatic heating/ cooling is responsible, tested by CTIPe model

Dr. Fuller-Rowell and Dr. Art Richmond

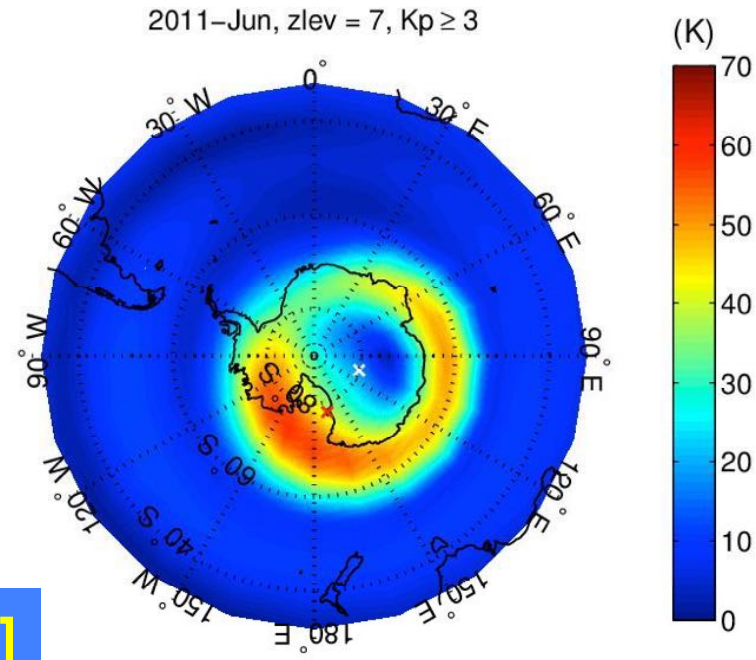

[Fong et al., GRL, 2015]

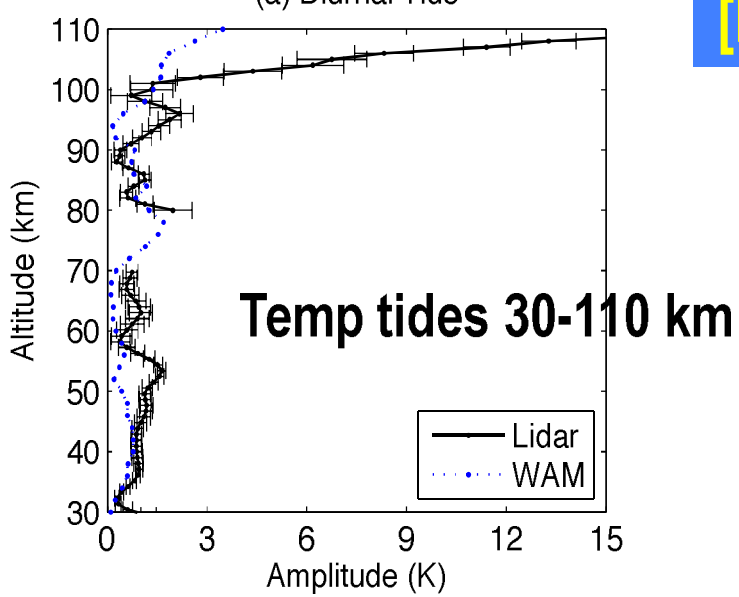

[Fong et al., JGR, 2014]

(a) Diurnal Amplitude at McMurdo

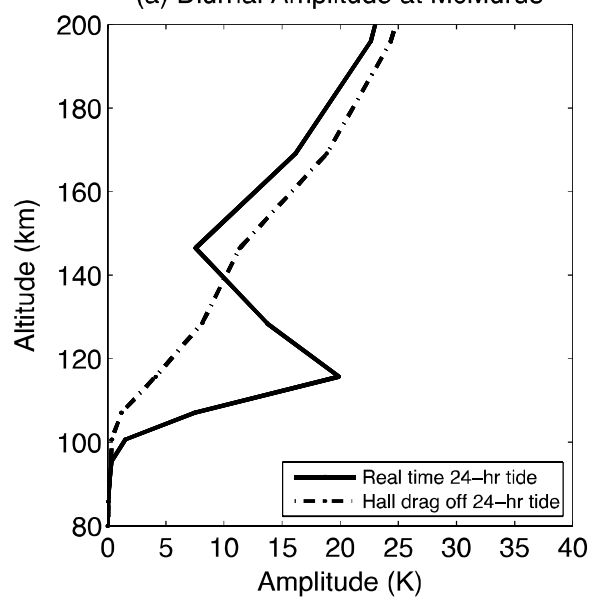

(b) Horizontal Wind Vector Difference

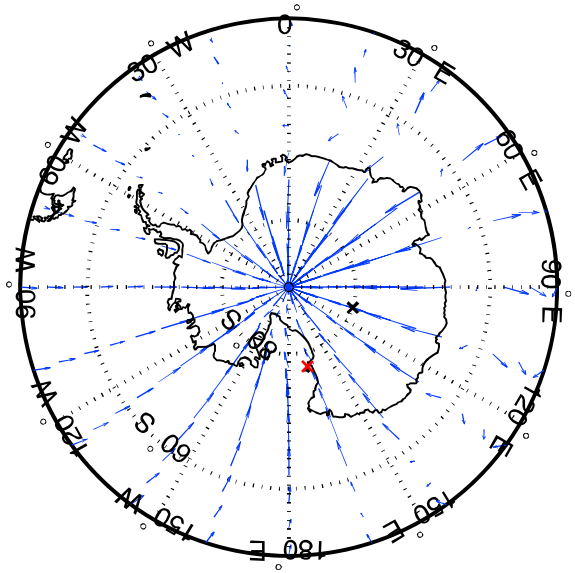

McMurdo Lidar Campaign (77.8°S, 166.7°E)

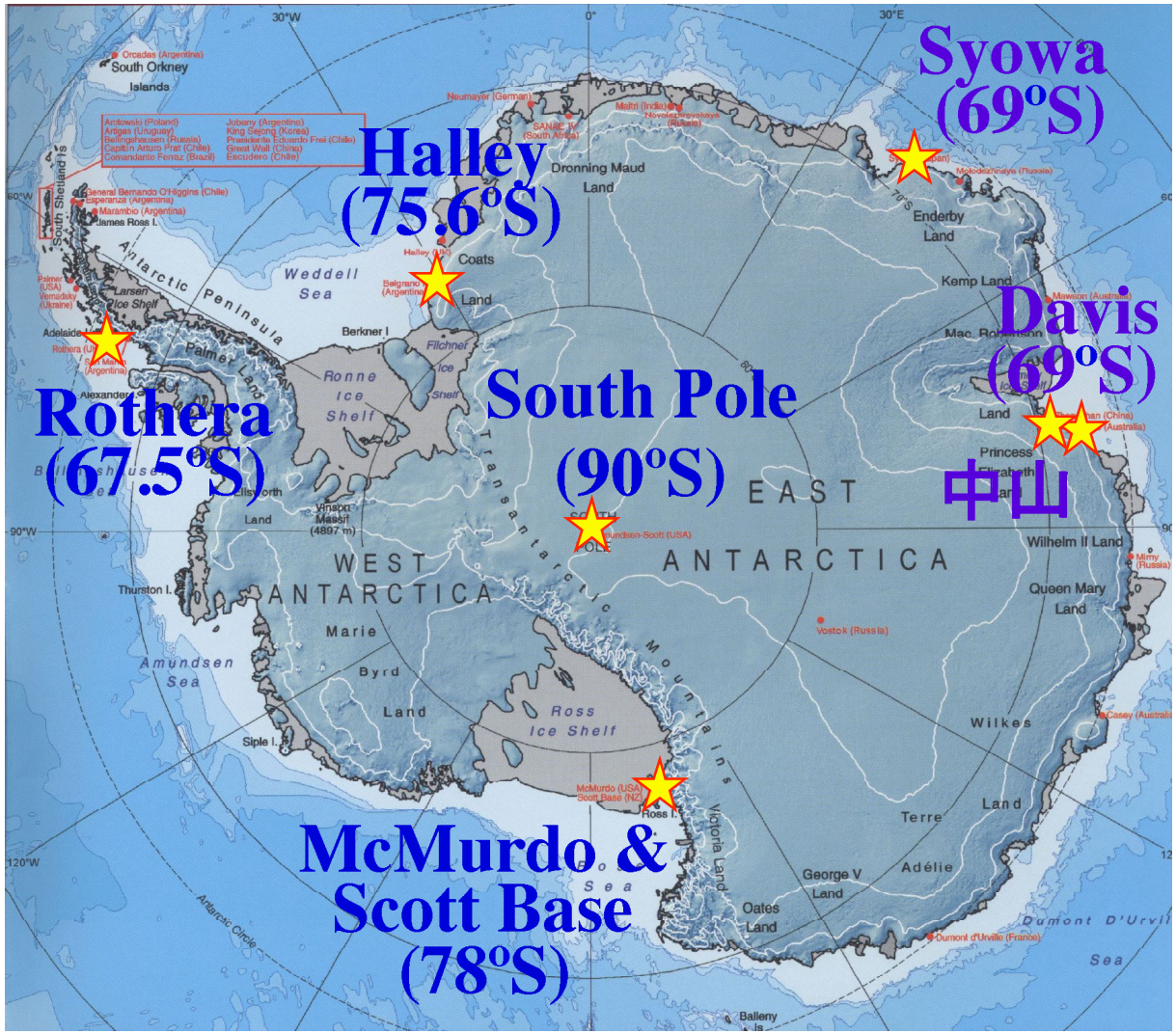

TIFe Layer

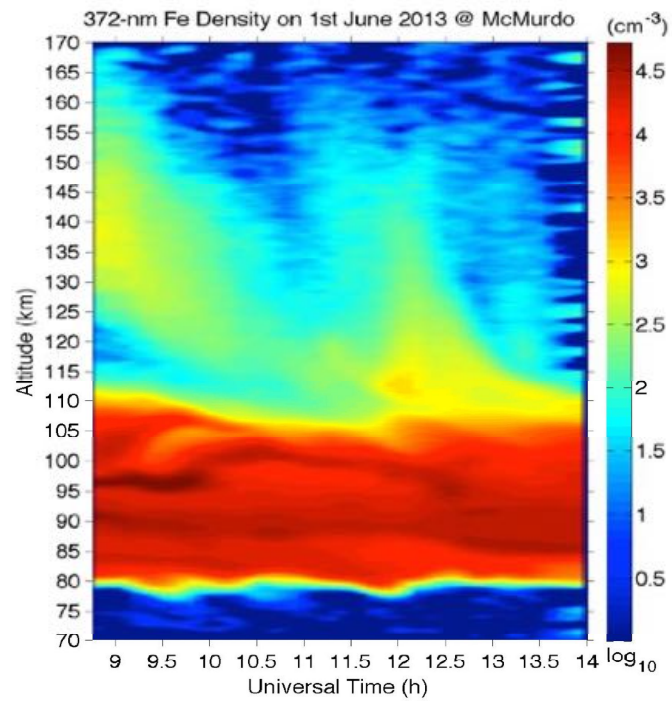

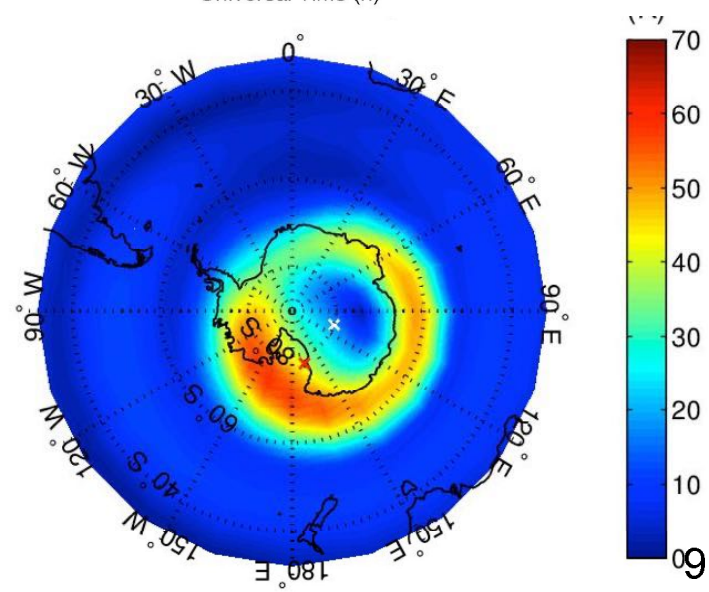

Many new discoveries from McMurdo lidar observations are transformative to advancing space-atmosphere sciences

Lidar Observations of Cosmic Dust

Preview

1. Thermospheric Fe layers observed to ~200 km open a new door to study the space-atmosphere interactions
2. "Finger-like" Fe layers are simulated by a Thermosphere-Ionosphere Fe and Fe^+ (TIFe) model
3. TIFe layers are coupled to the AIM system & solar wind

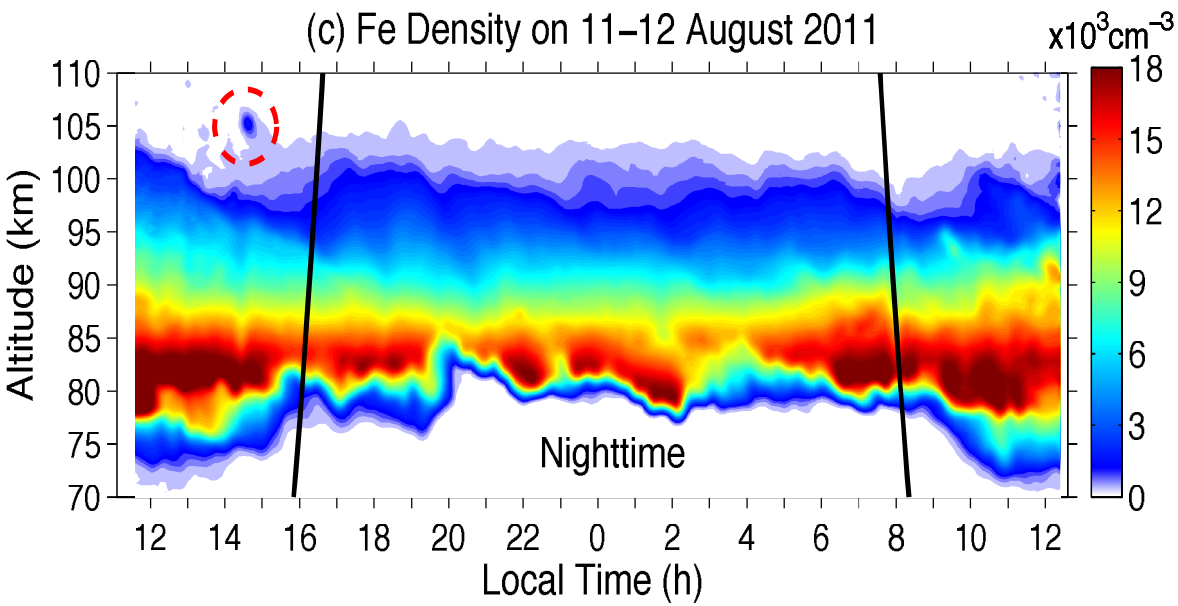

Fe density contour with a meteor trail at McMurdo [Yu *et al.*, JGR, 2012]

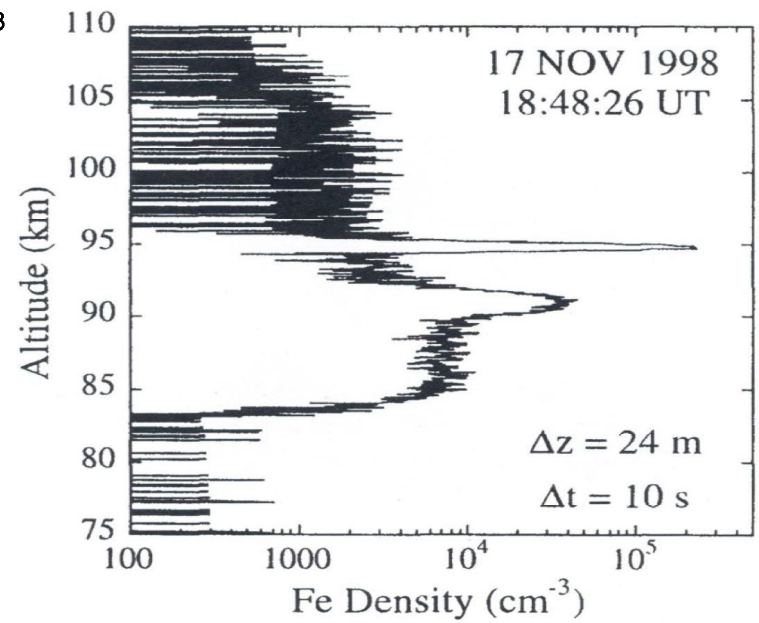

Profile on an Fe meteor trail measured by lidar [Chu *et al.*, GRL, 2000]

Still a big debate on the daily mass input of meteor to the Earth : from 5 to 300 tonnes.

Science discoveries from the McMurdo lidar campaign enable detection of neutral thermosphere with lidar

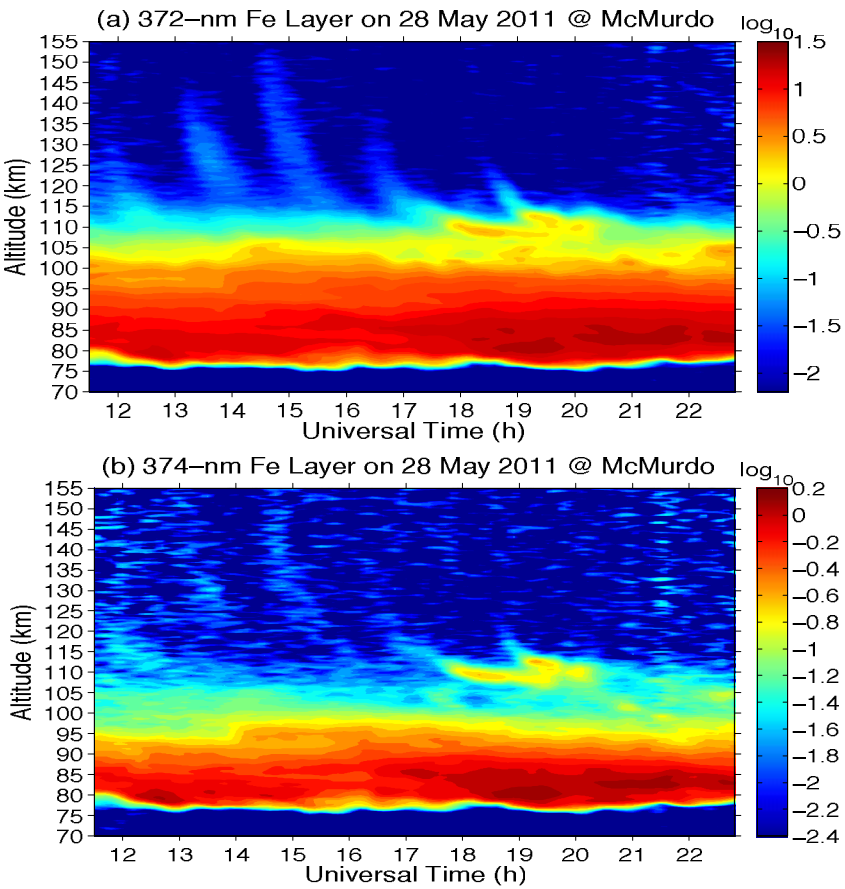

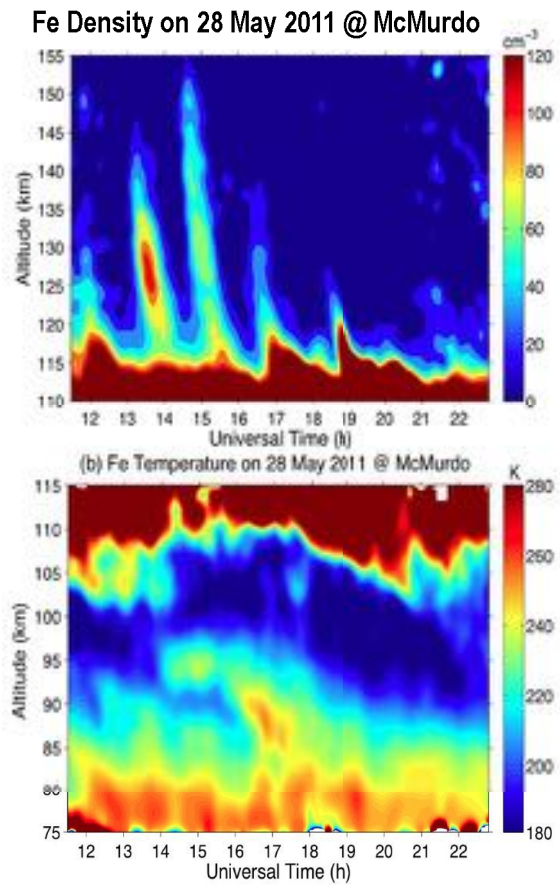

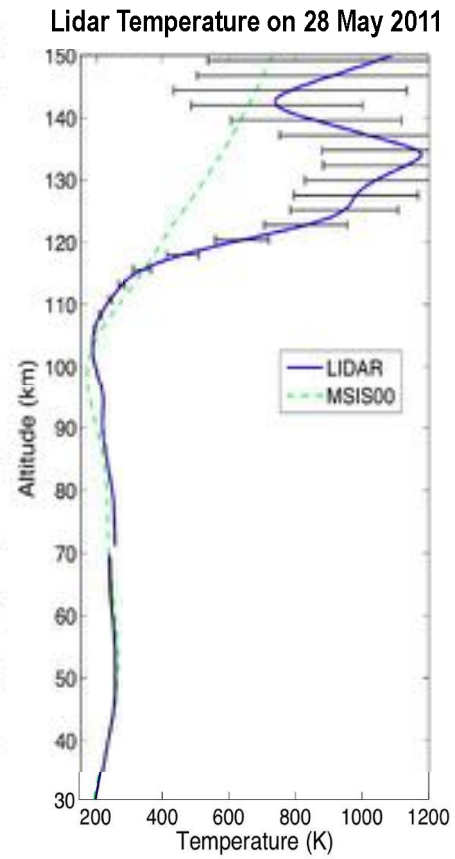

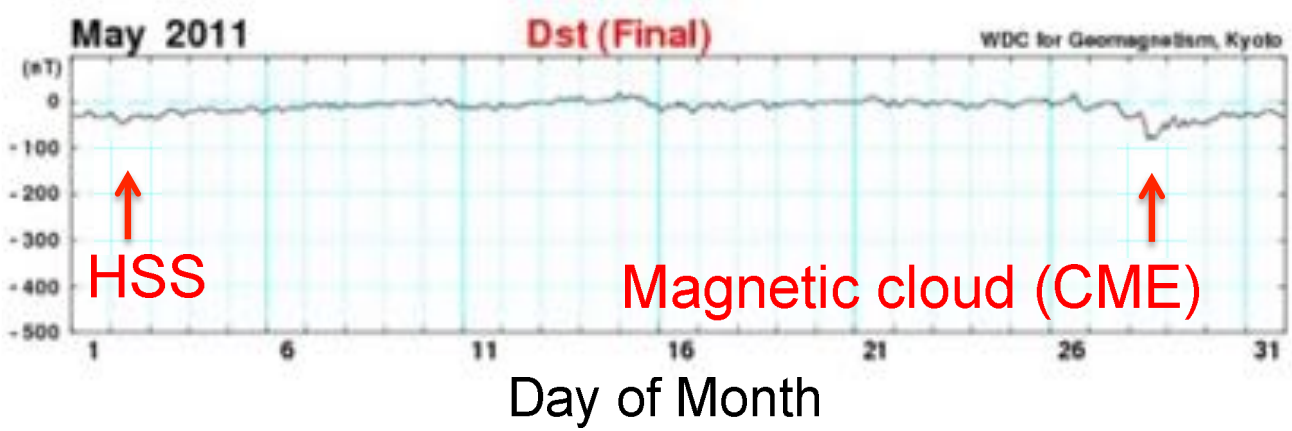

TIFe Layers on 28 May 2011

[Chu et al., GRL, 2011b]

Metal Layers are Excellent Tracers to Study the Fundamental Processes of A-I-M Coupling and SAIR

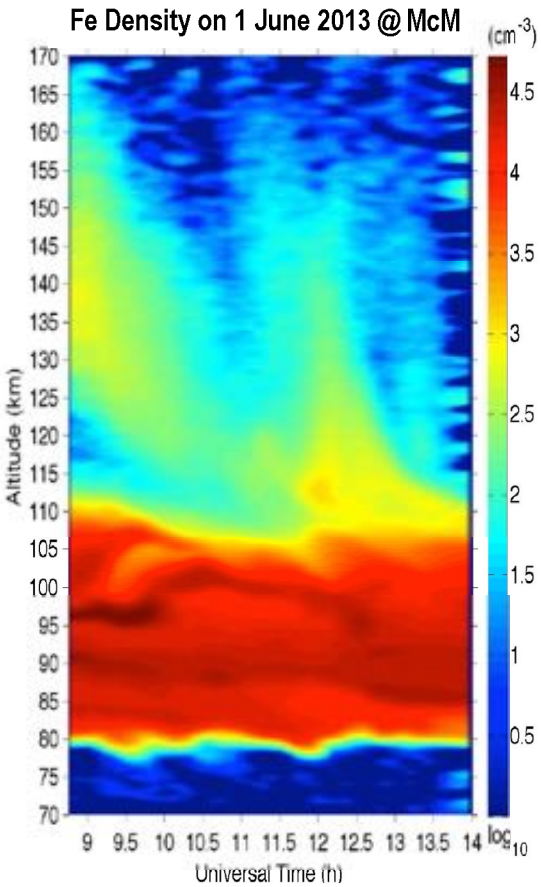

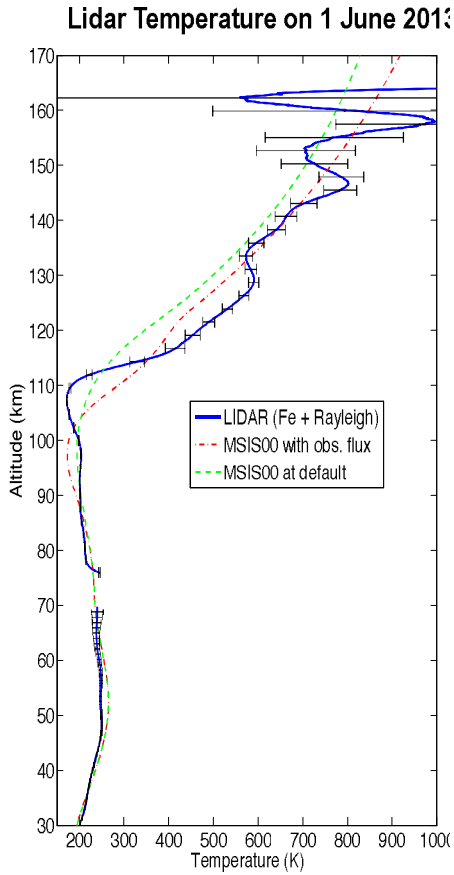

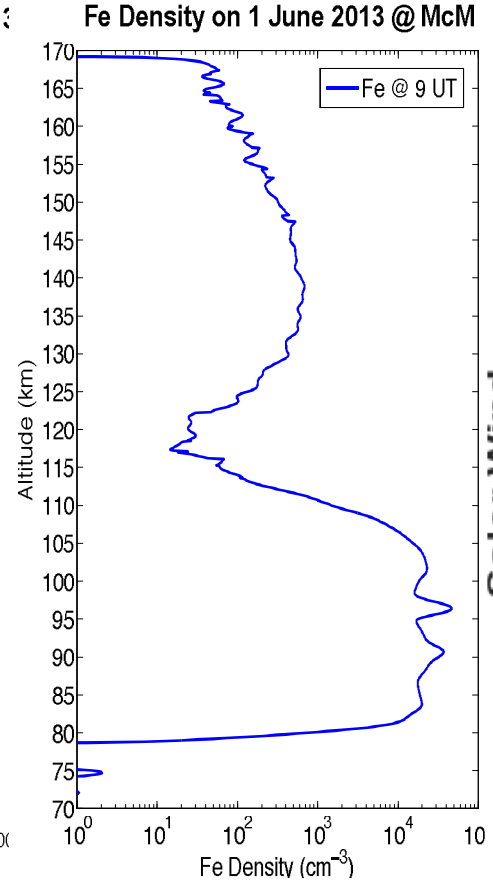

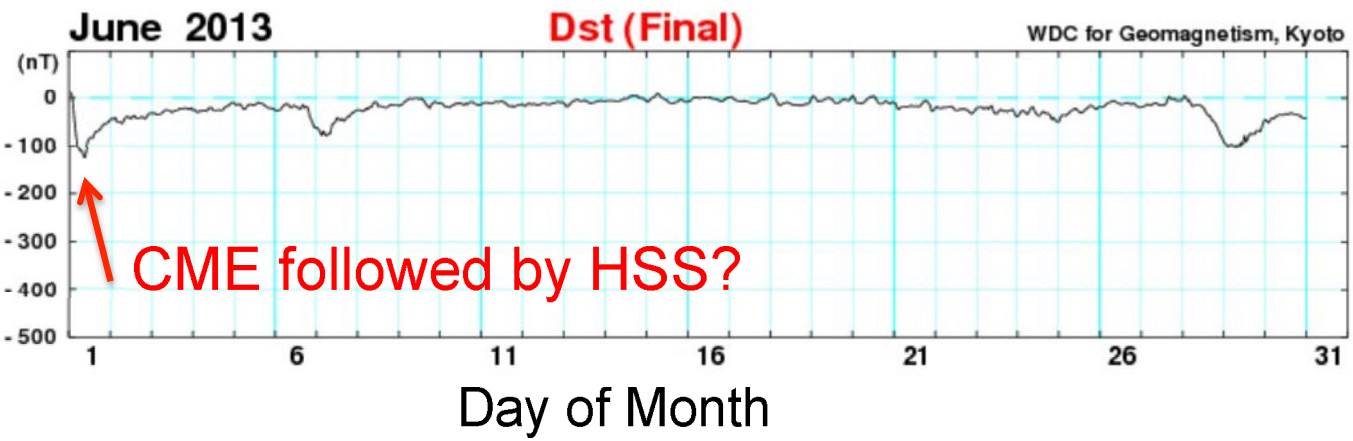

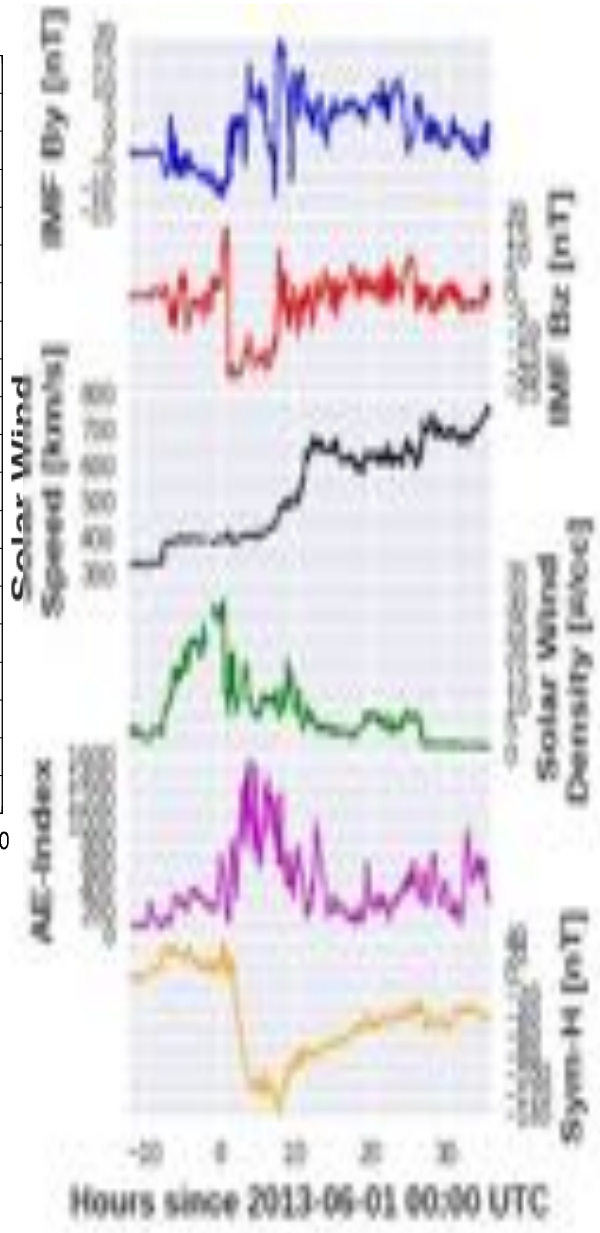

Overall Picture of TIFe Formation Mechanisms

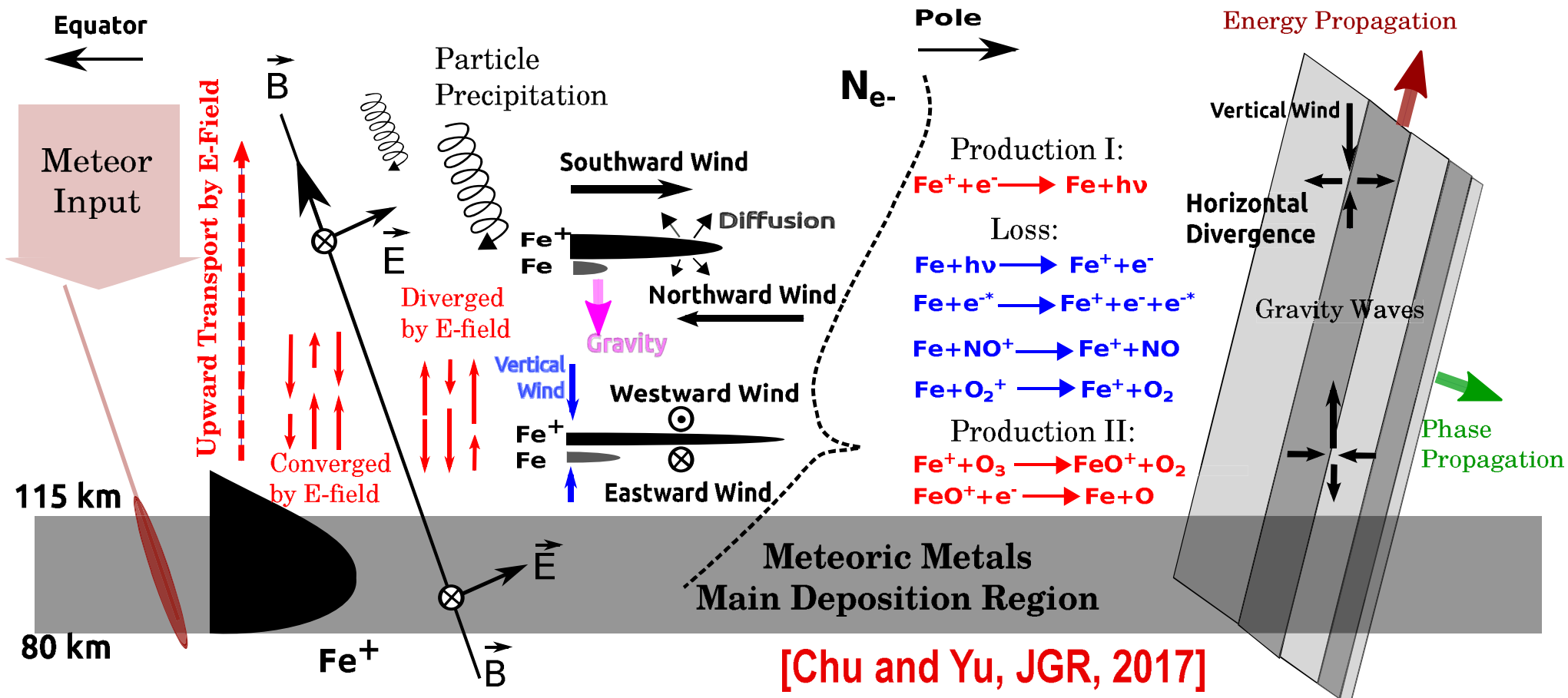

[Chu and Yu, JGR, 2017]

TIFe model formulates the TIFe theory depicting the lifecycle of meteoric metals via deposition, transport, chemistry, and wave dynamics. Meteor deposition mainly <115 km.

1) Upward transport of Fe^+ ions from the main deposition region by polar electric fields.

2) Convergence of Fe^+ ion layers in the E-F regions mainly by wave-induced wind shears.

3) Neutralization of Fe^+ ions to form Fe atoms mainly via **$Fe^+ + e^- \rightarrow Fe + h\nu$** above 120 km. Aurora particle precipitation helps the conversion from Fe^+ to Fe.

4) Evolution of Fe layer shapes under multiple factors: Gravity waves introduce vertical winds to transport Fe atoms in the thermosphere. Aurora particle precipitation enhances the TIFe layer contrast.

Choose to Model the TIFe Event on 28 May 2011

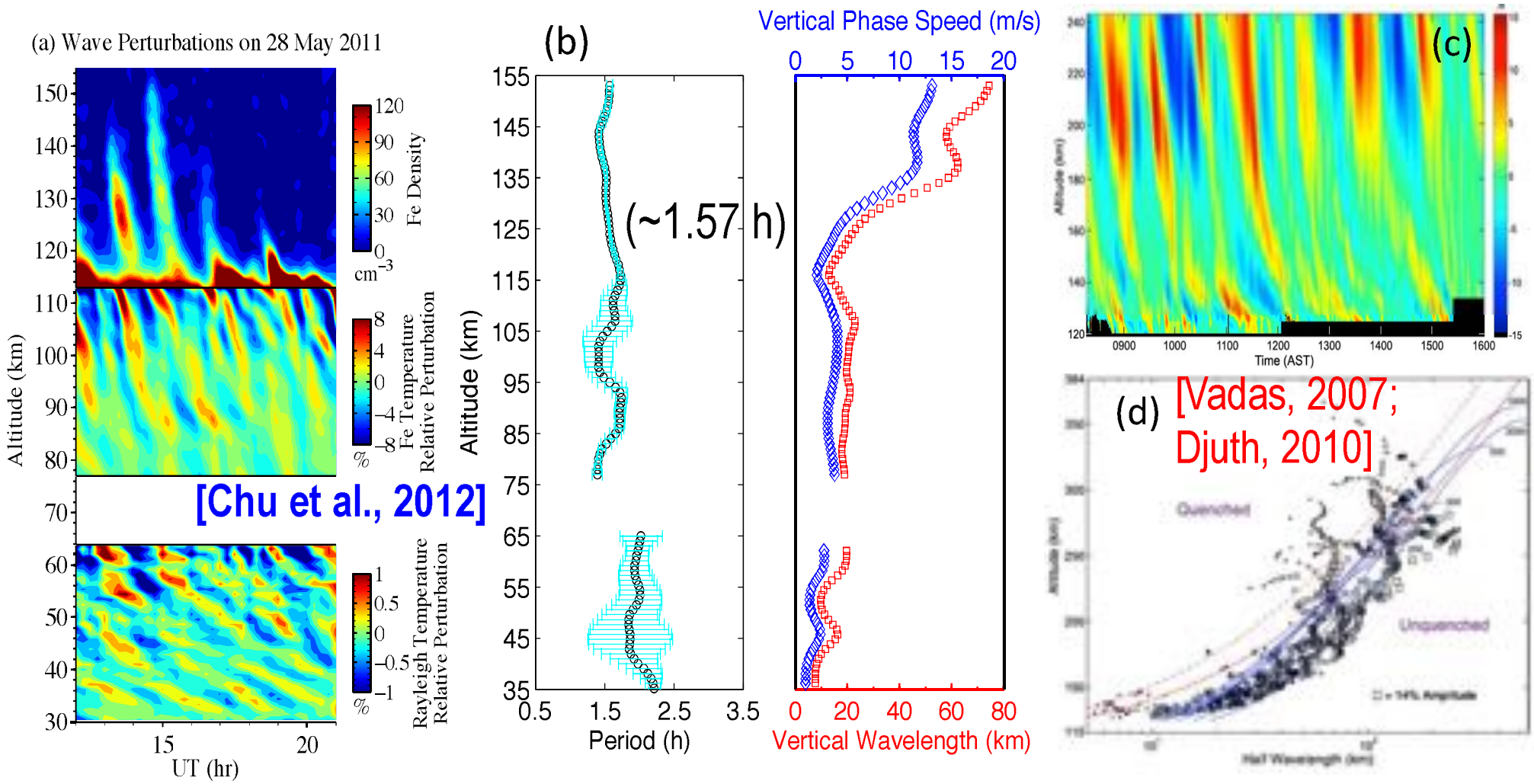

- Clear gravity wave signatures dominate the multiple TIFe layers with very high contrast.
- McMurdo TIFe layers and Arecibo TIDs have similar shapes. Both polar and low-latitude regions are associated with regions of upward plasma transport.
- A **coronal mass ejection (CME)** encountered the Earth as a **magnetic cloud** on 28 May 2011 according to Li et al. [2014].

IMF, Solar Wind, AE, Dst, Scott Base B-Field on 5/28/2011

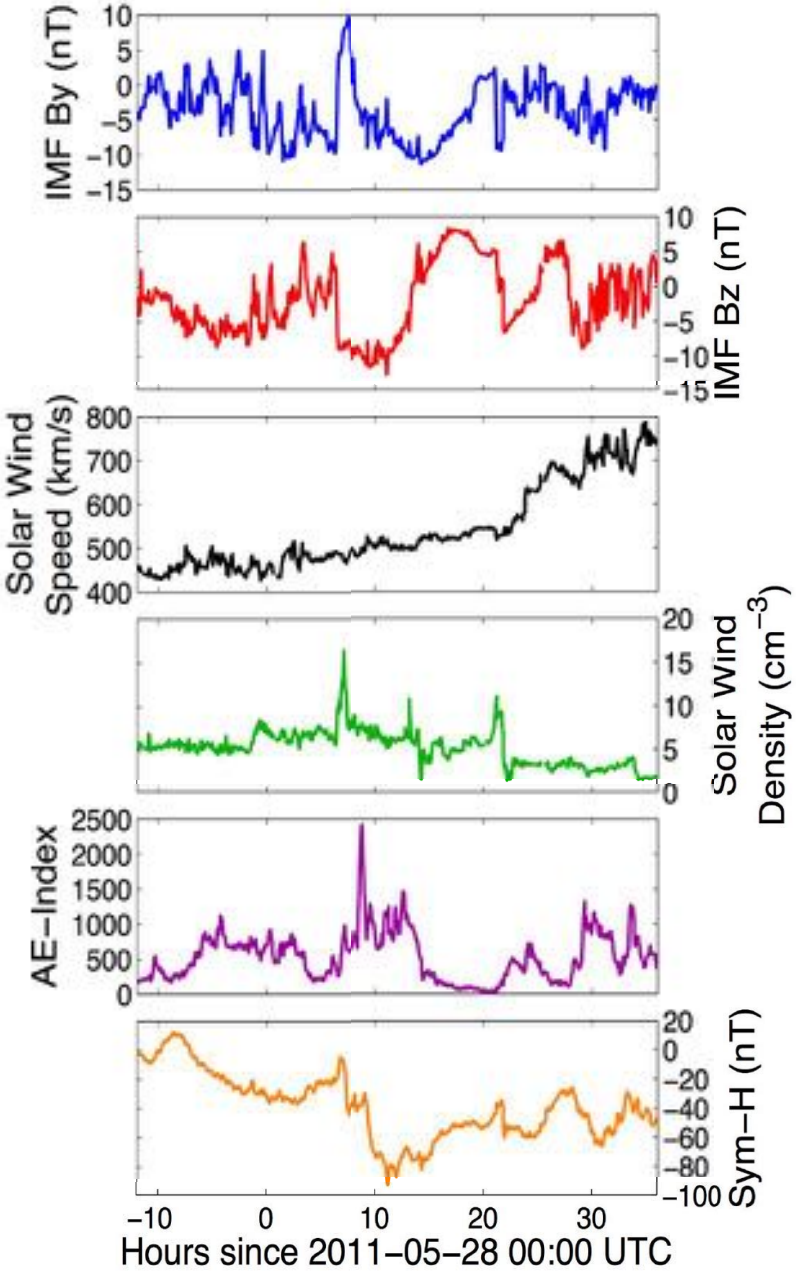

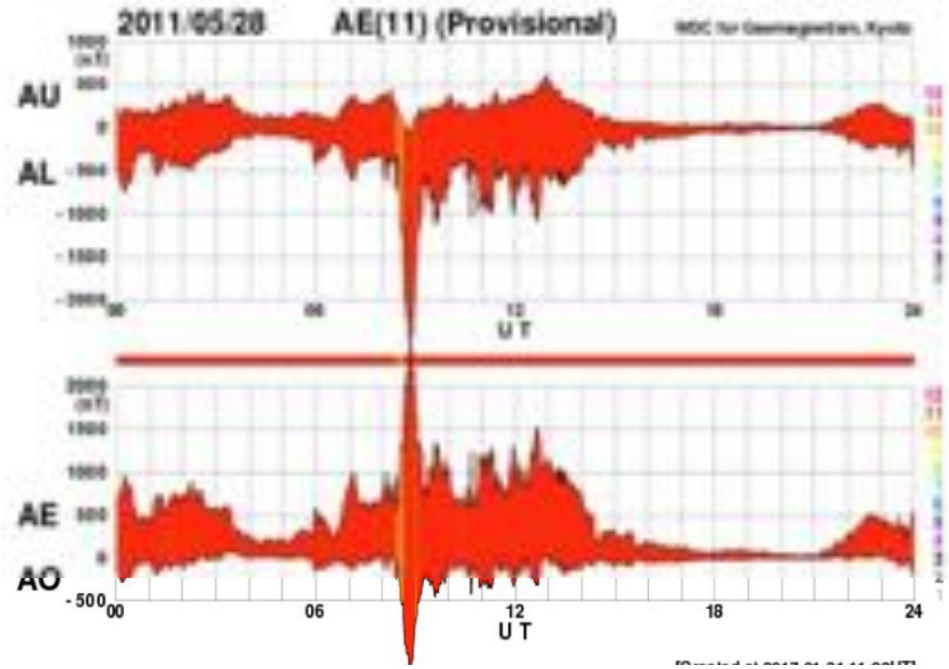

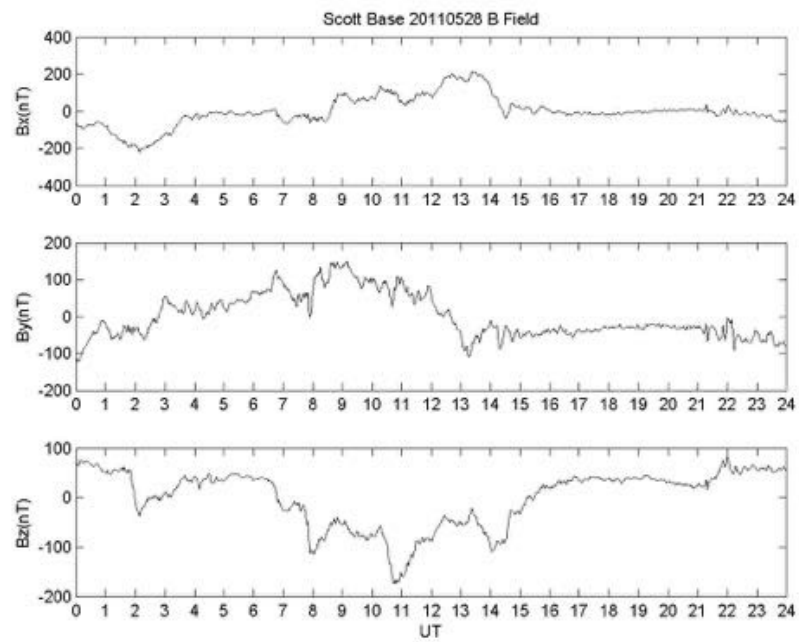

Scott Base Magnetometer

Courtesy of Liam Kilcommons and Dr. Zhonghua Xu for figures

Aurora Activity and Kp Index on 28 May 2011

Kp Index

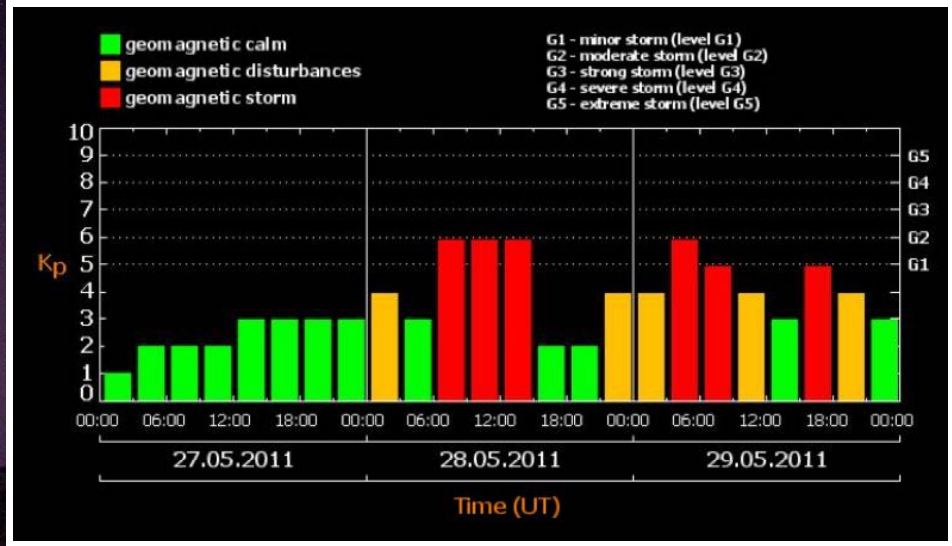

JHUAPL Ovation Model

http://sd-www.jhuapl.edu/Aurora/ovation/ovation_display.html

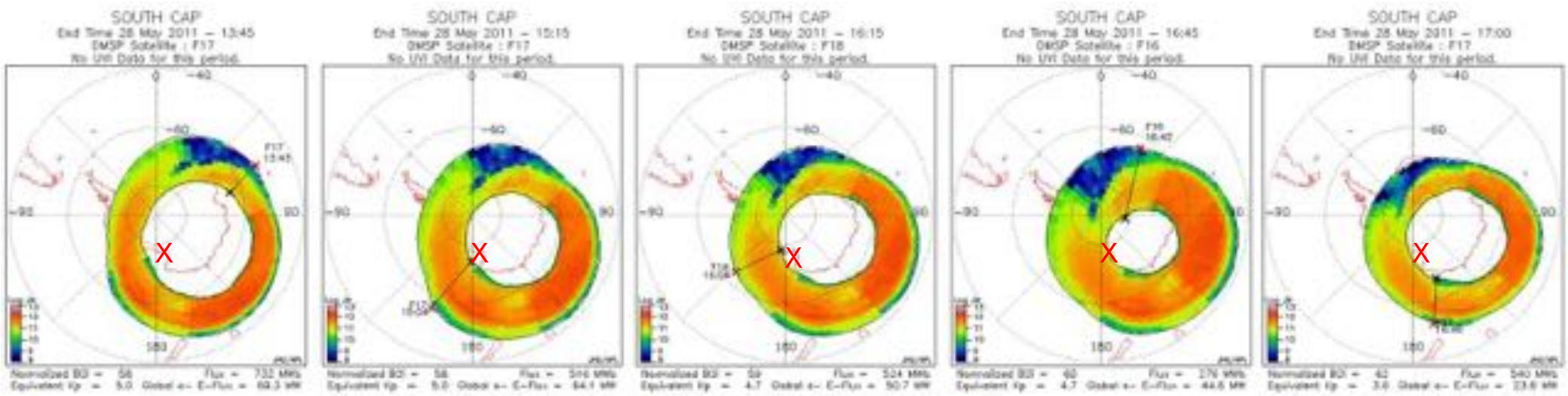

Courtesy of Dr. Zhonghua Xu for aurora figures

Thermosphere-Ionosphere Fe/Fe$^+$ (TIFe) Model

Based on a 3-D Math/Physics Model starting with the continuity equation

$$\frac{\partial N_M}{\partial t} = S + Q_M - L_M - \nabla \bullet \left(N_M \vec{V}_M \right)$$

Detailed development was done via a PhD Dissertation [Yu, 2014]
Further development and TIFe layer studies in [Chu and Yu, JGR, 2017]

Ultimate Source of Fe and Fe+ in the Mesosphere and Thermosphere

Extraterrestrial – meteoric deposition via ablation and sputtering of meteoroids

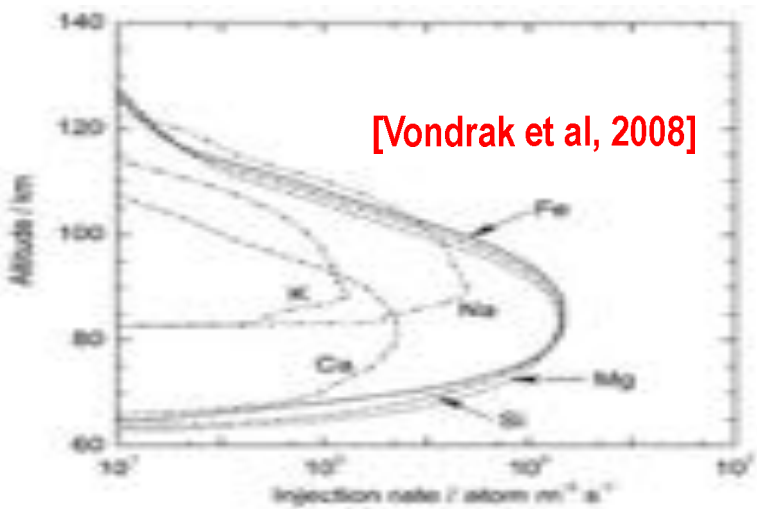

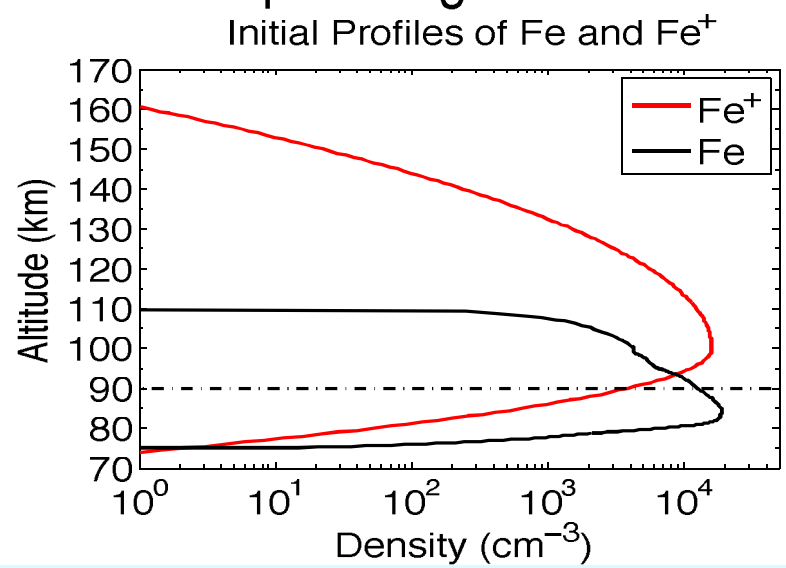

CABMOD [Carrillo-Sanchez et al., 2016] predicts 1.5, 0.28, 0.04 cm^{-3} @ 125, 150, 200 km, 2 orders of magnitude lower than the observed 120 and 20 cm^{-3} at 125 and 150 km. There would not be sufficient Fe or Fe+ densities at observed thermospheric altitudes if transport from the main layer were excluded.

Thermosphere-Ionosphere Fe/Fe⁺ (TIFe) Model

Chemical Production and Loss of Fe and Fe⁺ via Dynamical Reactions

Table 1. Neutral and Ionic Gas-Phase Chemistry of Iron Species (Fe and Fe^+) in the TIFe Model

Reaction Number	Reaction	Rate Coefficient[a]	Reference
R1	$Fe^+ + e^- \rightarrow Fe + h\nu$	$k_1 = 6.59\times10^{-12}(T/300)^{-0.50}$	*Nahar et al.* [1997]
R2	$Fe^+ + O_3 \rightarrow FeO^+ + O_2$	$k_2 = 7.07\times10^{-10}\exp(-129.9/T)$	*Rollason and Plane* [1998]
R3	$FeO^+ + e^- \rightarrow Fe + O$	$k_3 = 5.5\times10^{-7}\sqrt{298/T}$	*Bones et al.* [2016]
R4	$FeO^+ + O \rightarrow Fe^+ + O_2$	$k_4 = 3.2\times10^{-11}$	*Woodcock et al.* [2006]
R5	$Fe + h\nu \rightarrow Fe^+ + e^-$	$k_5 = 5\times10^{-7}[s^{-1}]$[b]	*Bautista et al.* [1998]
R6	$Fe + e^{-*} \rightarrow Fe^+ + e^- + e^{-*}$	See Text	*Shah et al.* [1993]
R7	$Fe + O_2^+ \rightarrow Fe^+ + O_2$	$k_7 = 1.1\times10^{-9}$	*Rutherford and Vroom* [1972]
R8	$Fe + NO^+ \rightarrow Fe^+ + NO$	$k_8 = 9.2\times10^{-10}$	*Rutherford and Vroom* [1972]
R9	$Fe + O_3 \rightarrow FeO + O_2$	$k_9 = 3.44\times10^{-10}\exp(-145.5/T)$	*Helmer and Plane* [1994]
R10	$FeO + O \rightarrow Fe + O_2$	$k_{10} = 4.6\times10^{-10}\exp(-350/T)$	*Self and Plane* [2003]
R11	$FeN_2^+ + O \rightarrow FeO^+ + N_2$	$k_{11} = 4.6\times10^{-10}$	*Woodcock et al.* [2006]
R12	$FeO_2^+ + O \rightarrow FeO^+ + O_2$	$k_{12} = 6.3\times10^{-11}$	*Woodcock et al.* [2006]
R13	$FeO_2^+ + e^- \rightarrow Fe + O_2$	$k_{13} = 3\times10^{-7}\sqrt{200/T}$	*Helmer et al.* [1998]
R14	$FeN_2^+ + e^- \rightarrow Fe + N_2$	$k_{14} = 3\times10^{-7}\sqrt{200/T}$	*Plane et al.* [1999]
R15	$Fe^+ + N_2 + M \rightarrow FeN_2^+ + M$	$k_{15} = 8.0\times10^{-30}(T/300)^{-1.52}$	*Woodcock et al.* [2006]
R16	$Fe^+ + O_2 + M \rightarrow FeO_2^+ + M$	$k_{16} = 1.7\times10^{-29}(T/300)^{-1.86}$	*Woodcock et al.* [2006]
R17	$FeN_2^+ + O_2 \rightarrow FeO_2^+ + N_2$	$k_{17} = 3.17\times10^{-10}$	*Vondrak et al.* [2006]
R18	$FeO + O_3 \rightarrow FeO_2 + O_2$	$k_{18} = 2.94\times10^{-10}\exp(-174.4/T)$	*Rollason and Plane* [2000]
R19	$FeO + O_2 + M \rightarrow FeO_3 + M$	$k_{19} = 4.41\times10^{-30}(T/200)^{0.606}$	*Rollason and Plane* [2000]
R20	$FeO_2 + O \rightarrow FeO + O_2$	$k_{20} = 1.4\times10^{-10}\exp(-580/T)$	*Self and Plane* [2003]
R21	$FeO_2 + O_3 \rightarrow FeO_3 + O_2$	$k_{21} = 4.4\times10^{-10}\exp(-170/T)$	*Self and Plane* [2003]
R22	$FeO_3 + O \rightarrow FeO_2 + O_2$	$k_{22} = 3.5\times10^{-10}\exp(-2386/T)$	*Self and Plane* [2003]
R23	$FeO_3 + H_2O \rightarrow Fe(OH)_2 + O_2$	$k_{23} = 5.0\times10^{-12}$	*Self and Plane* [2003]
R24	$FeO + H_2O + M \rightarrow Fe(OH)_2 + M$	$k_{24} = 5\times10^{-28}(200/T)^{1.13}$	*Rollason and Plane* [2000]
R25	$Fe(OH)_2 + H \rightarrow FeOH + H_2O$	$k_{25} = 1.1\times10^{-10}\exp(-300/T)$	*Jensen and Jones* [1974]
R26	$FeO_3 + H \rightarrow FeOH + O_2$	$k_{26} = 3\times10^{-10}\exp(-796/T)$	*Feng et al.* [2013]
R27	$FeOH + H \rightarrow Fe + H_2O$	$k_{27} = 2.0\times10^{-12}\exp(-600/T)$	*Jensen and Jones* [1974]
R28	$FeOH + H \rightarrow FeO + H_2$	$k_{28} = 5.0\times10^{-11}\exp(-800/T)$	*Jensen and Jones* [1974]
R29	$FeOH + FeOH \rightarrow (FeOH)_2$	$k_{29} = 9\times10^{-10}$	*Feng et al.* [2013]
R30	$FeOH + h\nu \rightarrow Fe + OH$	$k_{30} = 6\times10^{-3}[s^{-1}]$[b]	*Viehl et al.* [2016]
R31	$Fe + O^+ \rightarrow Fe^+ + O$	$k_{31} = 2.94\times10^{-9}$	*Rutherford and Vroom* [1972]
R32	$Fe + N^+ \rightarrow Fe^+ + N$	$k_{32} = 1.47\times10^{-9}$	*Rutherford and Vroom* [1972]
R33	$Fe + N_2^+ \rightarrow Fe^+ + N_2$	$k_{33} = 4.29\times10^{-10}$	*Rutherford and Vroom* [1972]
R34	$Fe + H^+ \rightarrow Fe^+ + H$	$k_{34} = 7.35\times10^{-9}$	*Rutherford and Vroom* [1972]

[a]The unit of rate coefficient is $cm^3\ s^{-1}$ for bimolecular reactions and $cm^6\ s^{-1}$ for termolecular reactions.
[b]When the solar elevation angle is below 0°, k_5 and k_{30} are zero.

Production

$$Fe^+ + e^- \rightarrow Fe + h\nu$$

$$Fe^+ + O_3 \rightarrow FeO^+ + O_2$$

$$FeO^+ + e^- \rightarrow Fe + O$$

$$FeO^+ + O \rightarrow Fe^+ + O_2$$

Loss

$$Fe + h\nu \rightarrow Fe^+ + e^-$$

$$Fe + e^{-*} \rightarrow Fe^+ + e^- + e^{-*}$$

$$Fe + O_2^+ \rightarrow Fe^+ + O_2$$

$$Fe + NO^+ \rightarrow Fe^+ + NO$$

$$Fe + O_3 \rightarrow FeO + O_2$$

$$FeO + O \rightarrow Fe + O_2$$

[Chu and Yu, JGR, 2017]

Thermosphere-Ionosphere Fe/Fe$^+$ (TIFe) Model

Transport (3-D) of Fe$^+$ and Fe, and Treatment in 1-D TIFe Model

$$q\vec{E}+q\vec{V}_i\times\vec{B}+m_i\nu_{in}\left(\vec{V}_n-\vec{V}_i\right)+m_i\vec{g}-\frac{\nabla P_i}{N_i}=0$$

$$\vec{V}_{Fe}=\vec{V}_n+\vec{V}_g+\vec{V}_d$$

$$\vec{V}_i=\frac{1}{1+\xi^2}\frac{\vec{E}\times\vec{B}}{B^2}+\frac{q(\vec{E}\bullet\vec{B})}{m_i\nu_{in}B^2(1+\xi^2)}\vec{B}+\frac{\xi}{1+\xi^2}\frac{\vec{E}}{B}$$

$$+\frac{\xi}{1+\xi^2}\frac{\vec{V}_n\times\vec{B}}{B}+\frac{1}{1+\xi^2}\frac{(\vec{V}_n\bullet\vec{B})}{B^2}\vec{B}+\frac{\xi^2}{1+\xi^2}\vec{V}_n$$

$$+\frac{\vec{F}_i\times\vec{B}}{qB^2(1+\xi^2)}+\frac{(\vec{F}_i\bullet\vec{B})}{m_i\nu_{in}B^2(1+\xi^2)}\vec{B}+\frac{\xi}{qB(1+\xi^2)}\vec{F}_i$$

Ion motion

- By the electric field
- By the neutral winds
- By gravity and diffusion

[Yu, 2014]

Parameterize horizontal divergence

$$\nabla\bullet\left(N_M\vec{V}_M\right)=\nabla_h\bullet\left(N_M\vec{V}_{M,h}\right)+\frac{\partial\left(N_M V_{M,z}\right)}{\partial z}$$

$$\nabla_h\cdot\vec{V}_{i,h}\approx\left(\frac{\cos^2\Theta_D}{1+\xi^2}\frac{k_y^2}{k_x^2+k_y^2}+\frac{\xi^2}{1+\xi^2}\right)\nabla_h\cdot\vec{V}_{n,h}$$

$$\nabla_h\cdot\vec{V}_{n,h}=\frac{gV_{n,z}-C_s^2\frac{\partial V_{n,z}}{\partial z}}{C_s^2-\frac{\omega^2}{k_h^2}}$$

Gratefully acknowledge Dr. Art Richmond for his guidance

Thermosphere-Ionosphere Fe/Fe$^+$ (TIFe) Model

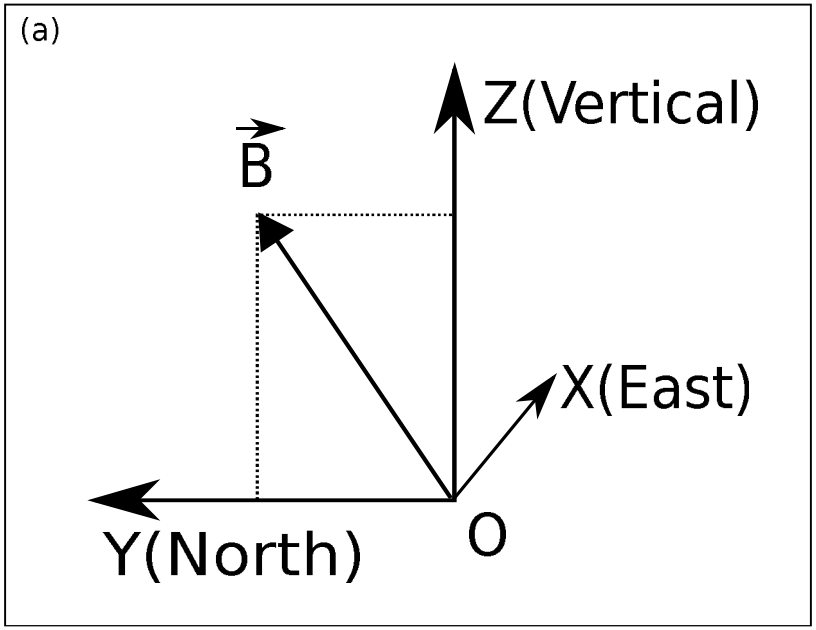

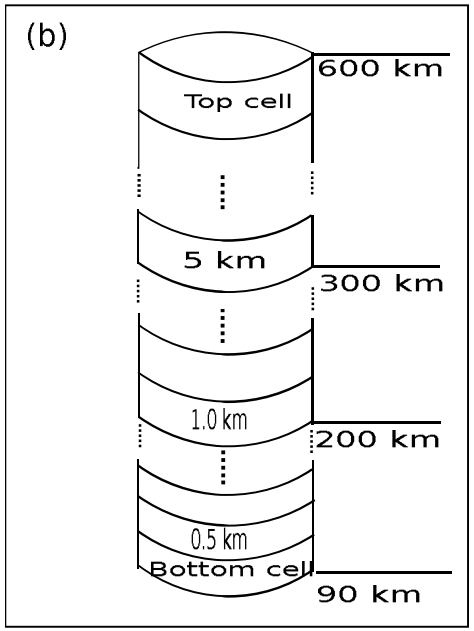

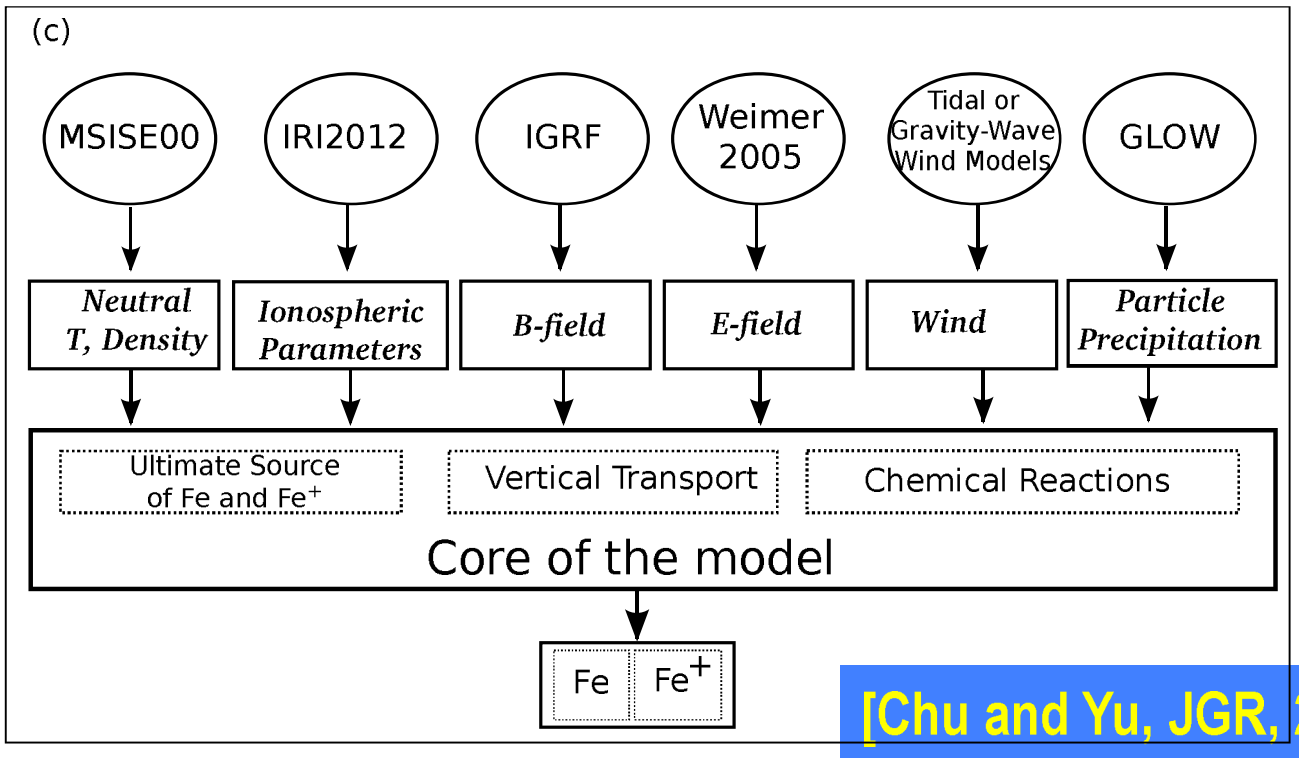

Geomagnetic coordinates in the frame fixed to the Earth's surface

1-D numerical model along vertical lidar beam Built upon a 3-D mathematical & physical model

Not self-consistent but taking inputs of neutrals, ionosphere, B- and E-fields, neutral wind, and particle precipitation from external models or data

[Chu and Yu, JGR, 2017]

Fe^+ Transport by Polar Electric Field

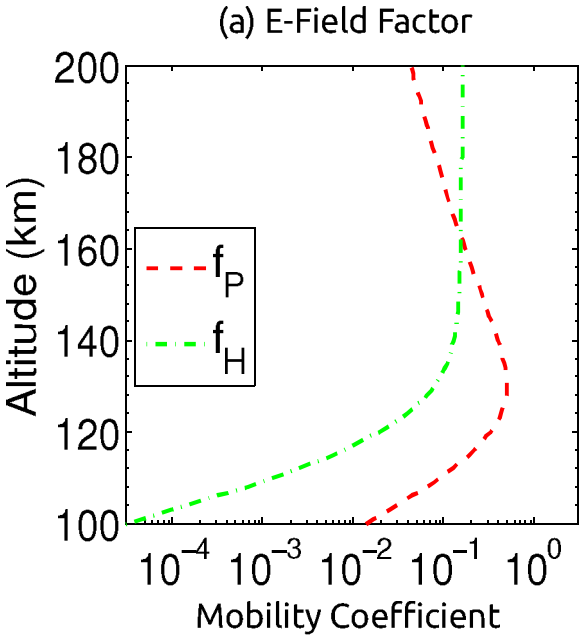

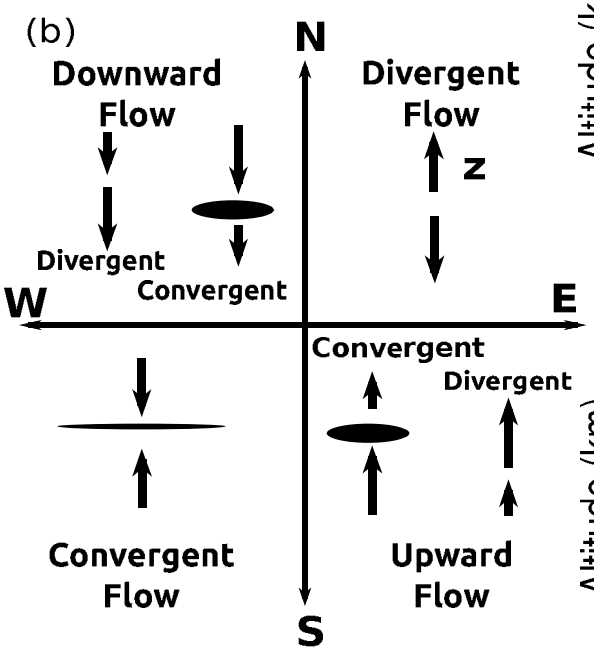

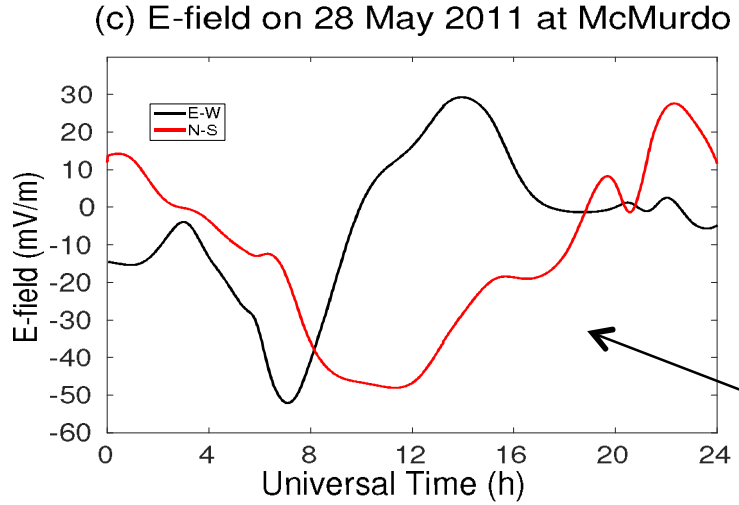

$$V_{ize} = \frac{\cos\Theta_D}{1+\xi^2}\frac{E_x}{B_0} + \frac{\xi}{1+\xi^2}\frac{E_z}{B_0}$$

$$= f_H \frac{E_x}{B_0} + f_P \frac{E_z}{B_0}$$

Weimer-2005 model (Dynamo ignored)

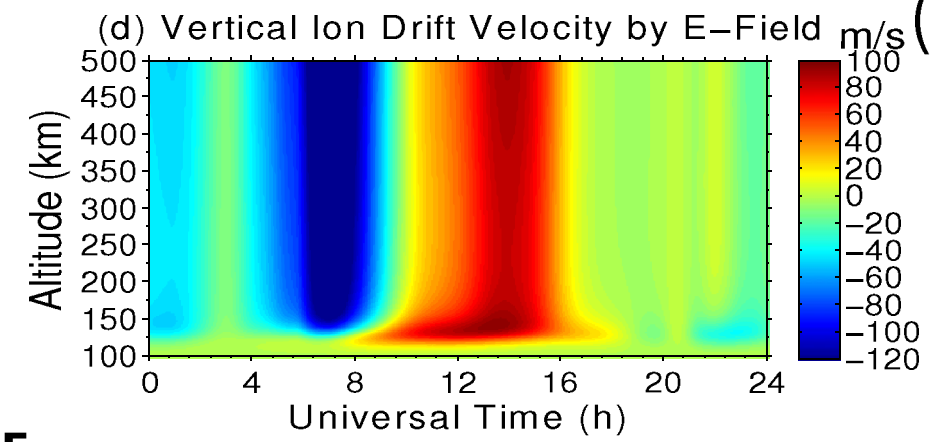

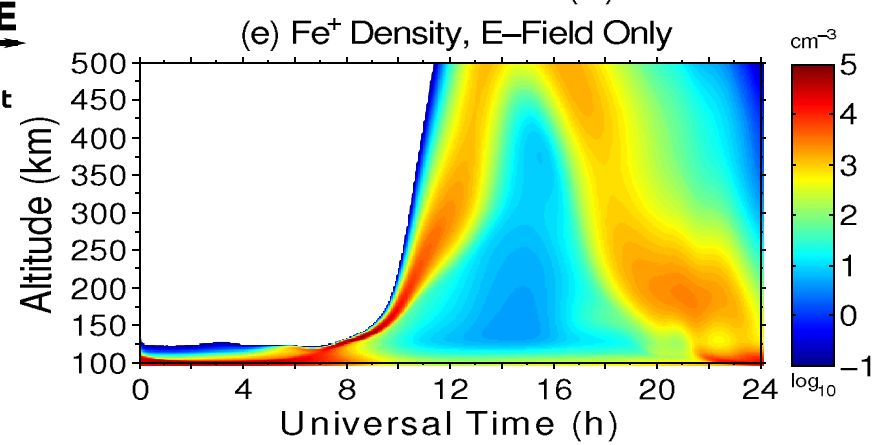

Fe^+ Transport by Neutral Winds

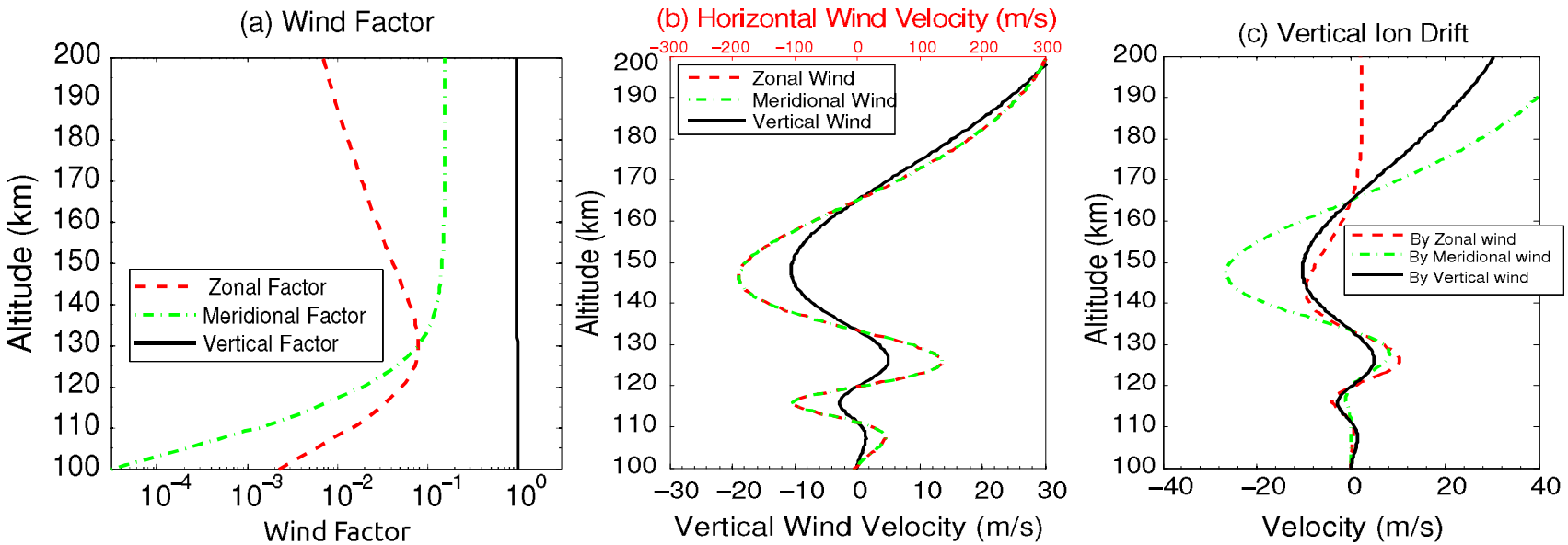

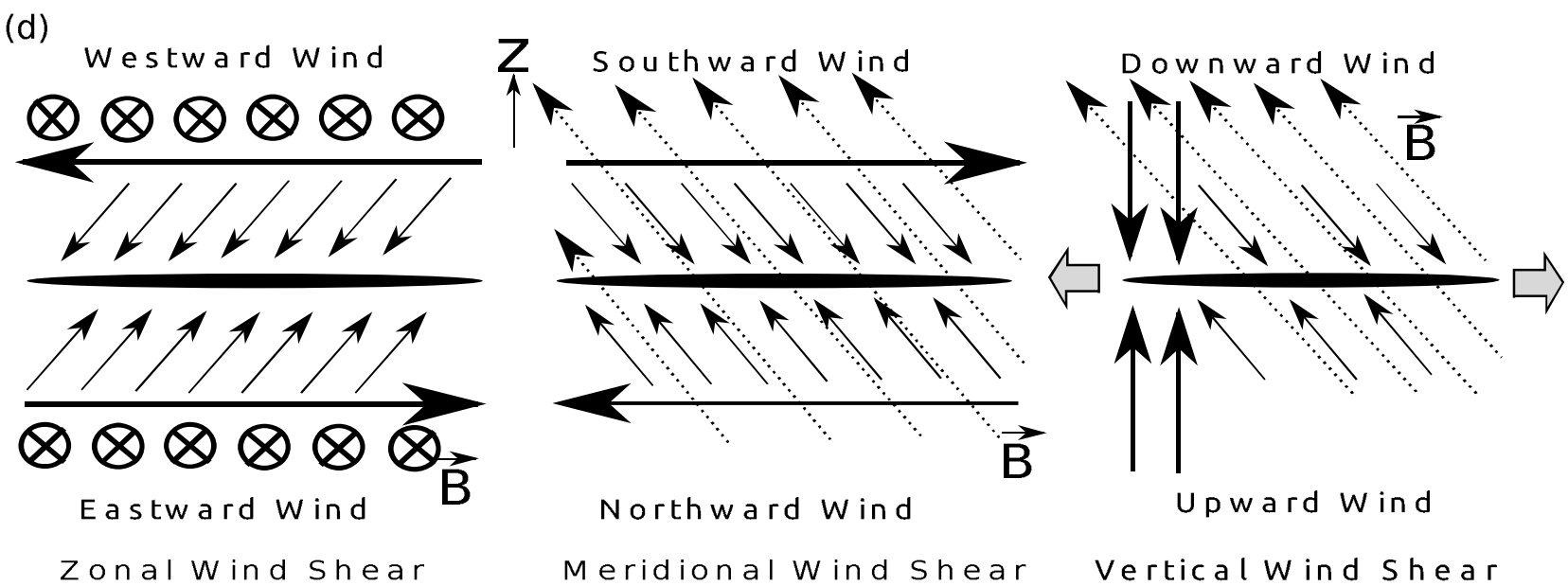

$$V_{izw} = \frac{\xi \cos\Theta_D}{1+\xi^2} V_{n,x} - \frac{\sin\left(2\Theta_D\right)}{2\left(1+\xi^2\right)} V_{n,y} + \left(1 - \frac{\cos^2\Theta_D}{1+\xi^2}\right) V_{n,z}$$

Fe^+ and Fe Transport by E-Field and Winds

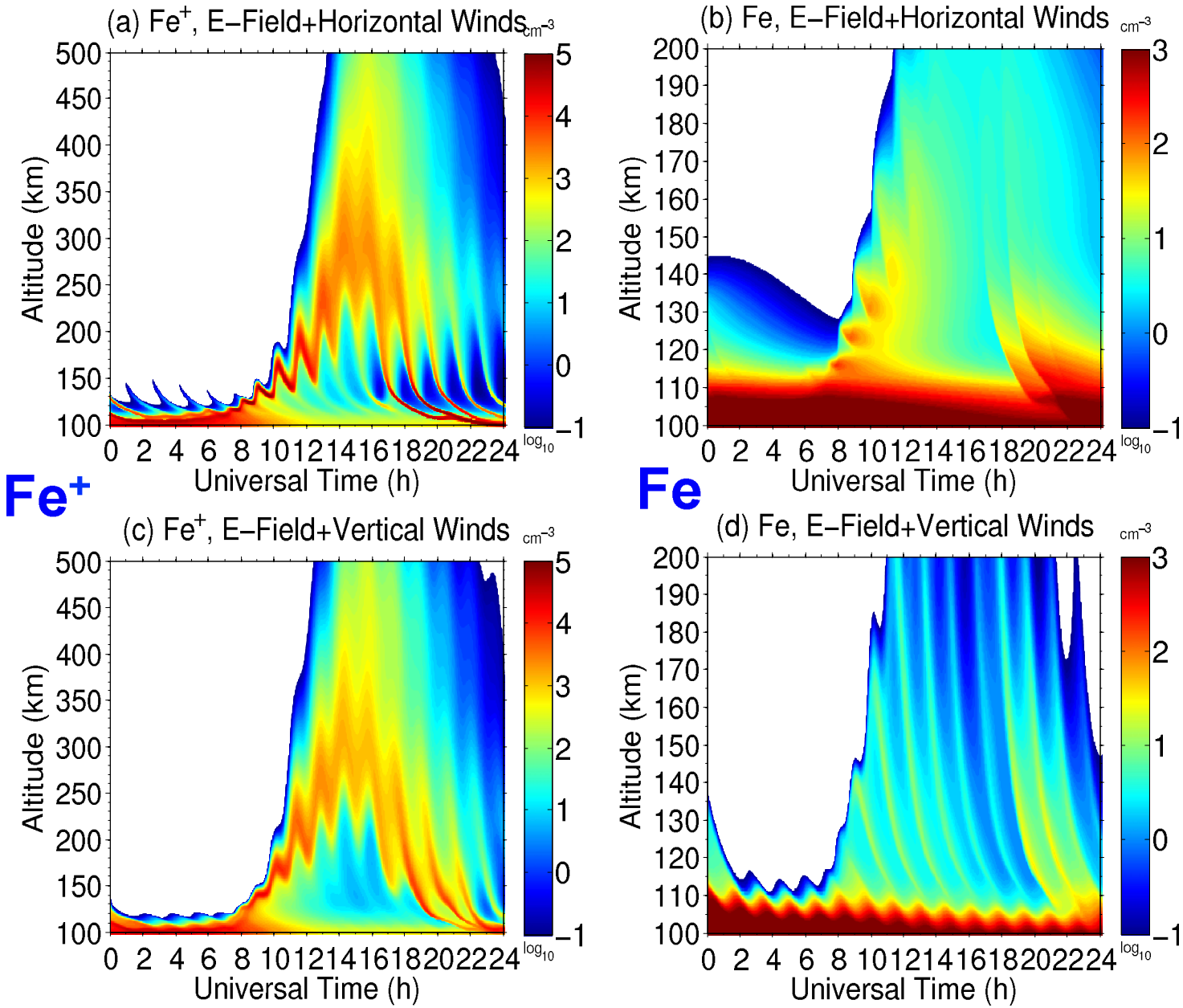

With Horizontal Winds

With Vertical Winds

GW-induced vertical winds are a key to shape the TIFe layers.

Fe and Fe^+ Chemistry: Direct vs. Dissociative Recomb.

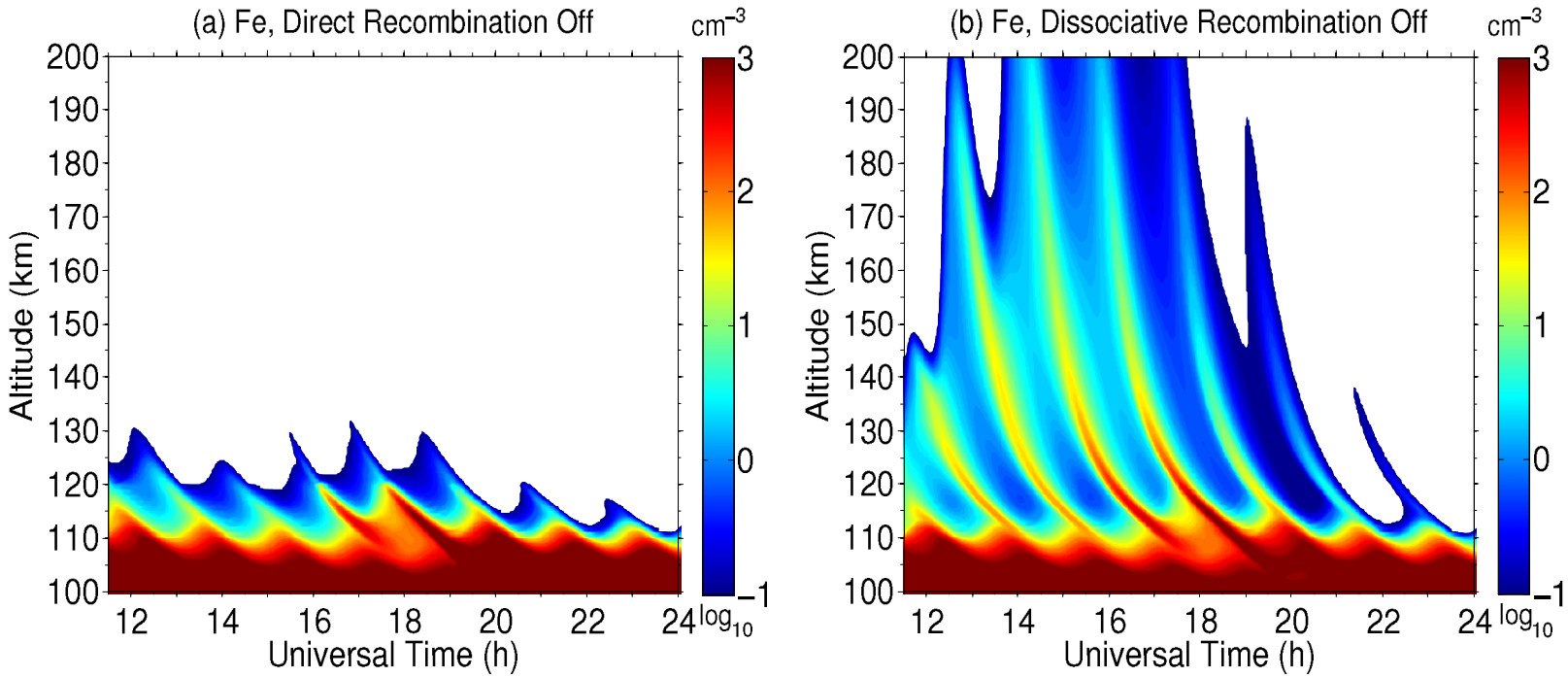

CA = (Fe, Fe+, FeO, FeO^+, FeO_2, FeO_2^+, FeO_3, FeN_2^+, FeOH, $Fe(OH)_2$, NO^+, O_2^+, O^+, N_2^+, N^+, and N).

16 minor species are modeled in TIFe chemical module

34 chemical reactions of Fe and Fe^+ minor species

26 chemical reactions of molecular ions

Direct recombination is the major channel to neutralize Fe^+ above ~120 km. Below it, dissociative recombination is effective and more factors play roles because of frequent ion-neutral collisions.

Fe and Fe$^+$ Chemistry: Impacts of Aurora Activity

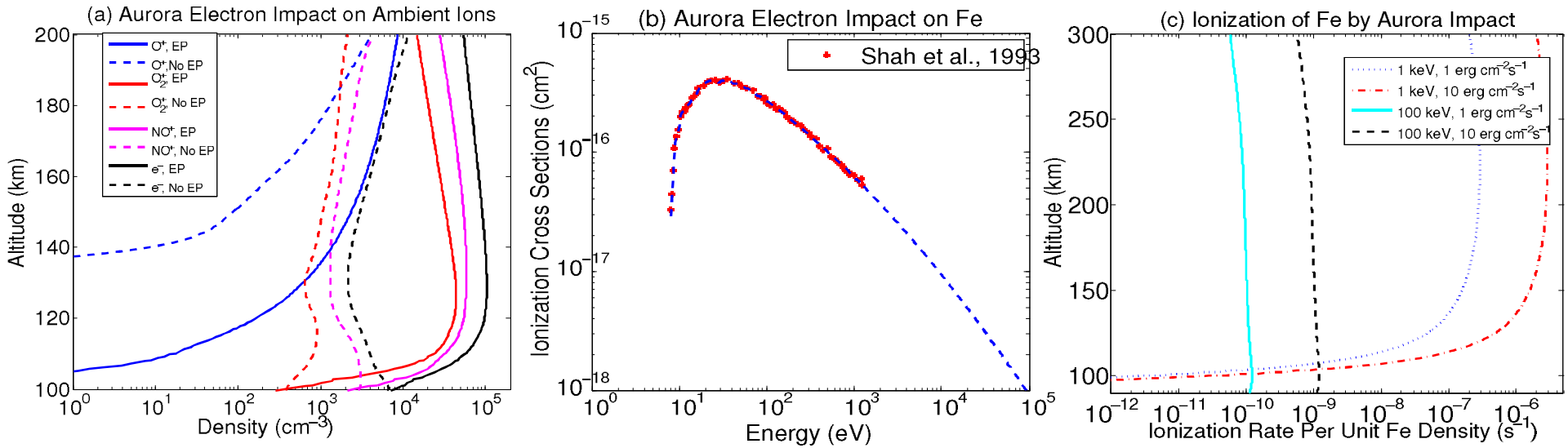

Energetic electron precipitation from aurora enhances Fe$^+$ neutralization by increasing [e$^-$].

When Fe and Fe$^+$ layers are decoupled, the lack of Fe production leads to a net loss of Fe via charge transfer with NO$^+$ and O$_2^+$. This net loss of Fe can be enhanced by an increase in NO$^+$ and O$_2^+$ densities due to aurora particle precipitation.

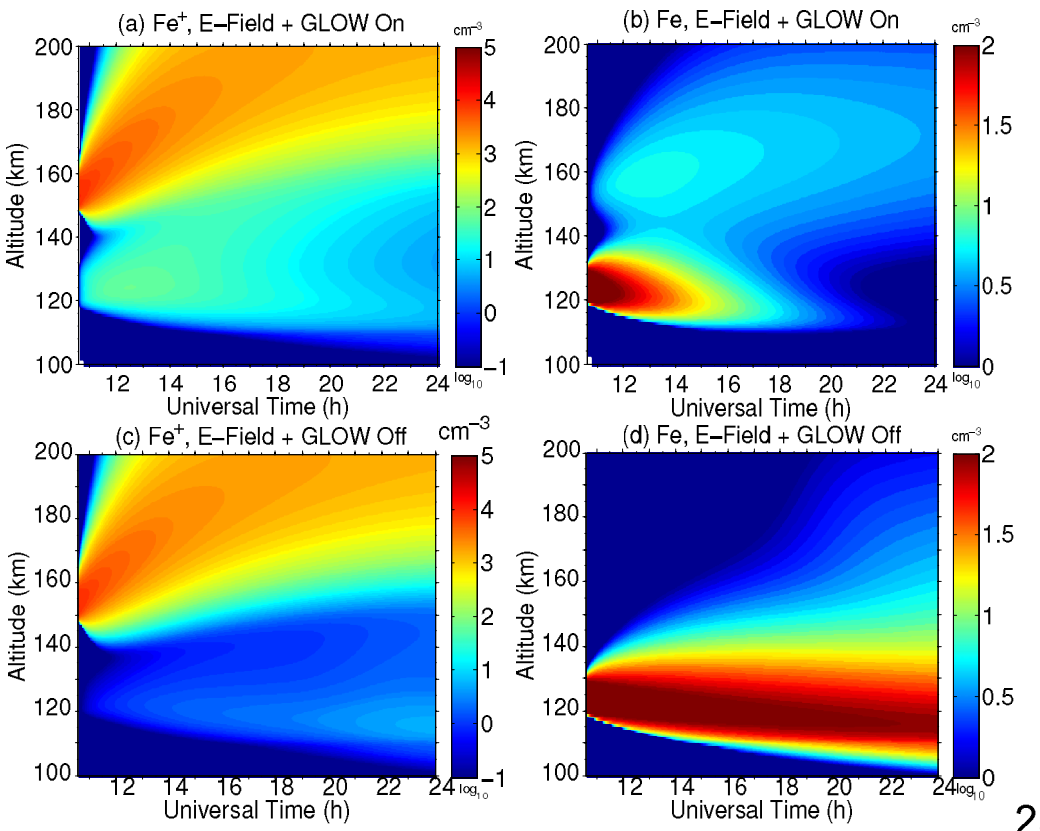

TIFe Model Simulations of 28 May 2011 Event

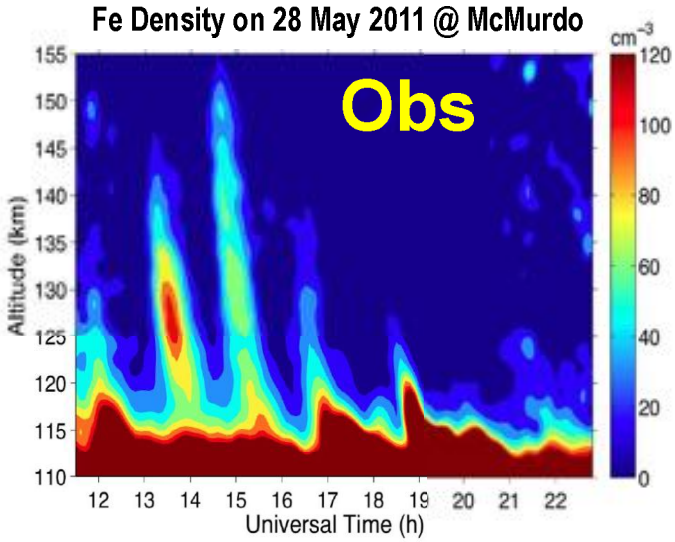

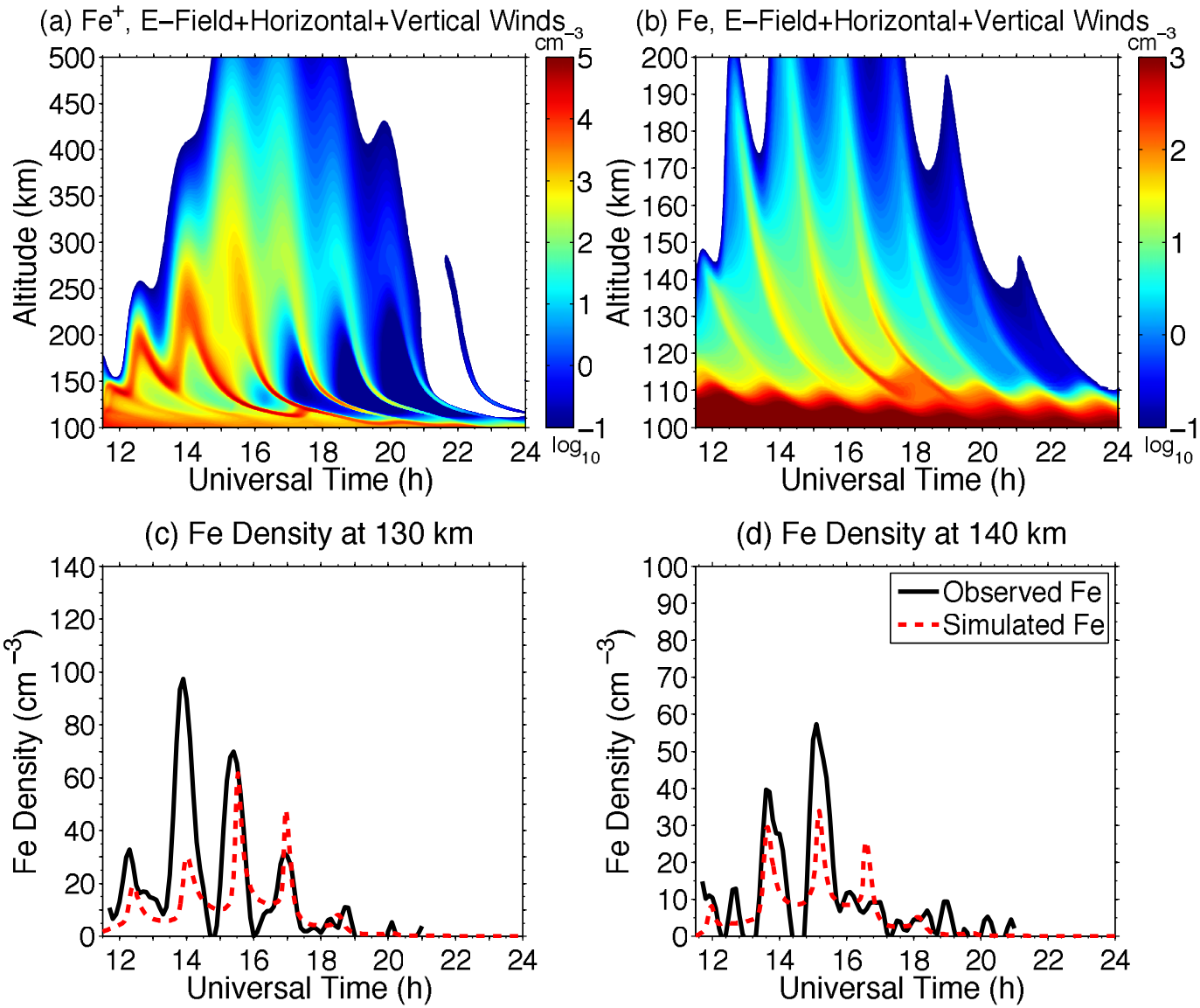

Initial Fe$^+$/Fe profiles
Full chemistry
45% E-field from Weimer-2005
Full horizontal divergence
GLOW model is on with 1.5
Zero background wind
Forward-modeled gravity wave induced horizontal and vertical winds

Energy influx to GLOW model is 1.5 erg/s/cm^2

[Chu and Yu, JGR, 2017]

TIFe Model with Enhanced Particle Precipitation

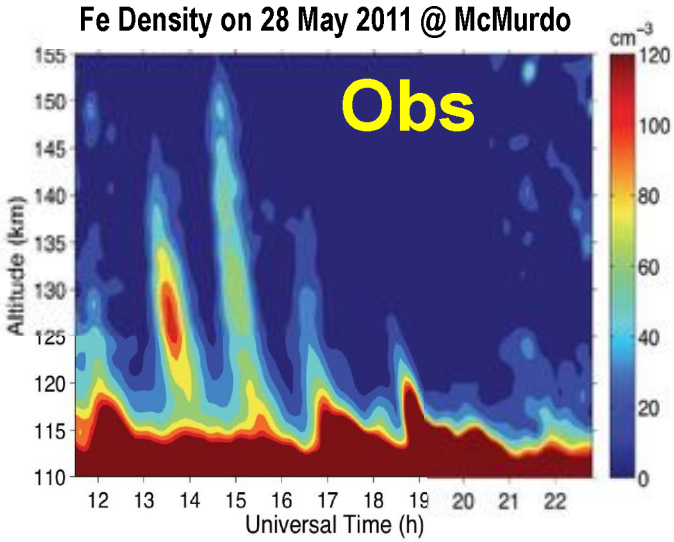

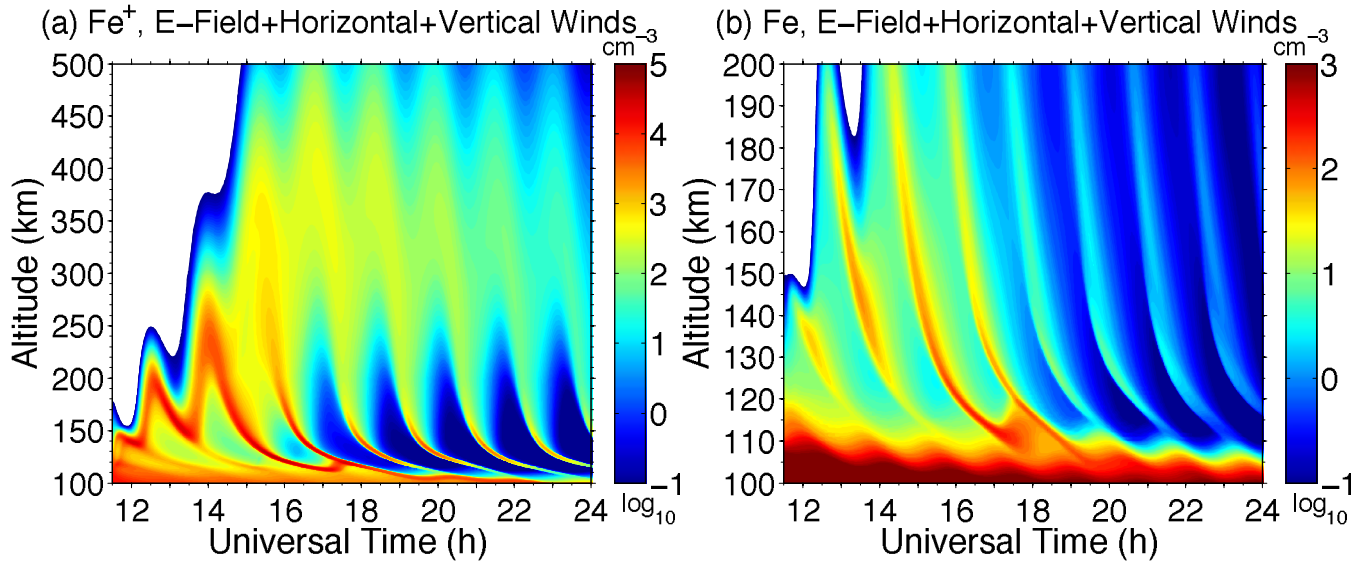

Initial Fe$^+$/Fe profiles
Full chemistry
45% E-field from Weimer-2005
Full horizontal divergence
GLOW model is on with 30
Zero background wind
Forward-modeled gravity wave induced horizontal and vertical winds

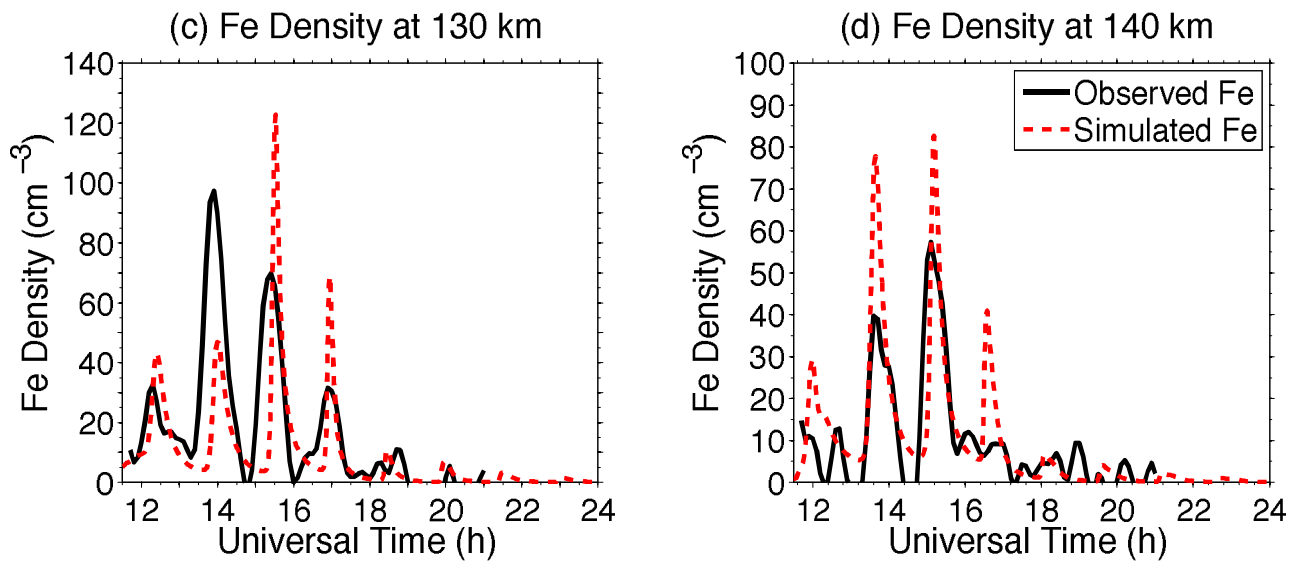

30 erg/s/cm^2

Localized particle precipitation, with much higher flux than the statistical distribution, can significantly improve the TIFe layer contrast

Overall Picture of TIFe Formation Mechanisms

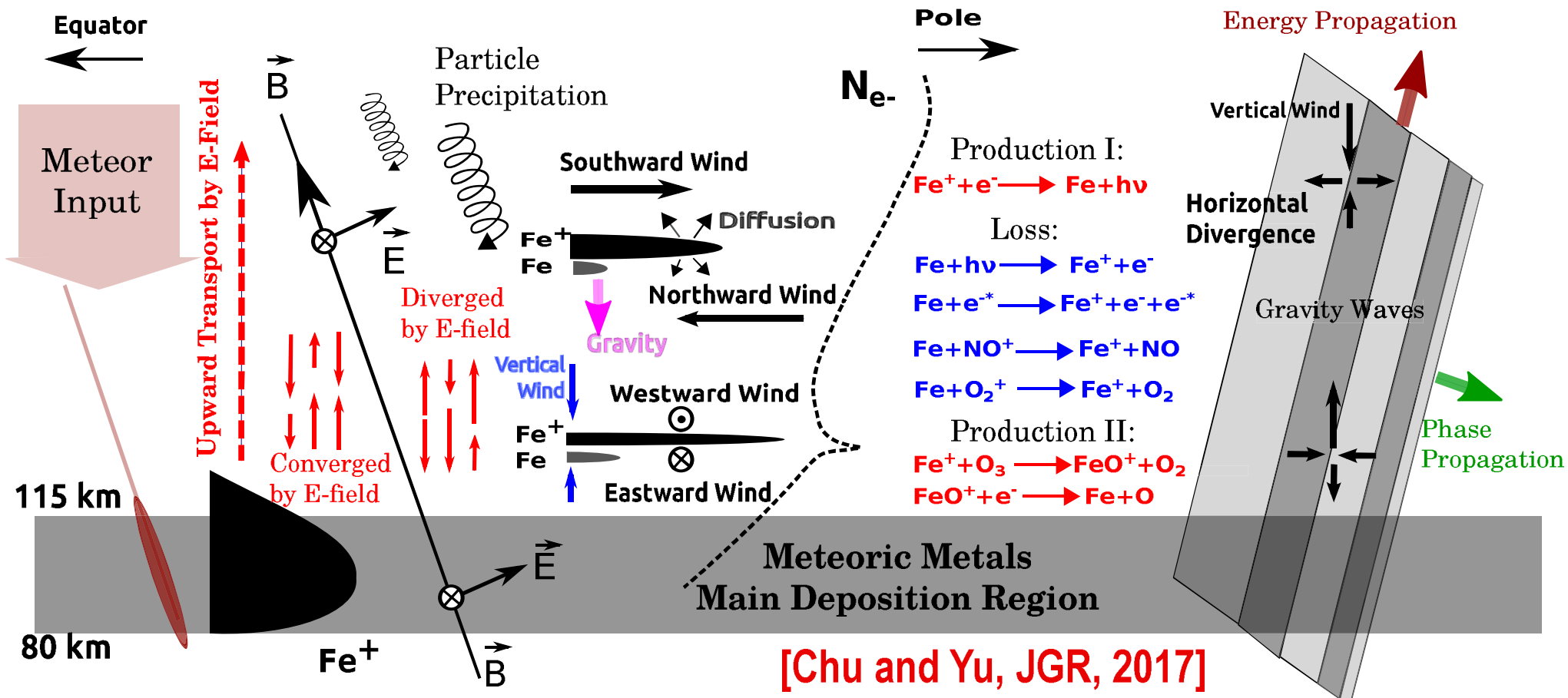

[Chu and Yu, JGR, 2017]

TIFe model formulates the TIFe theory depicting the lifecycle of meteoric metals via deposition, transport, chemistry, and wave dynamics. Meteor deposition mainly <115 km.

1) Upward transport of Fe^+ ions from the main deposition region by polar electric fields.

2) Convergence of Fe^+ ion layers in the E-F regions mainly by wave-induced wind shears.

3) Neutralization of Fe^+ ions to form Fe atoms mainly via **$Fe^+ + e^- \rightarrow Fe + h\nu$** above 120 km. Aurora particle precipitation helps the conversion from Fe^+ to Fe.

4) Evolution of Fe layer shapes under multiple factors: Gravity waves introduce vertical winds to transport Fe atoms in the thermosphere. Aurora particle precipitation enhances the TIFe layer contrast.

Solar Eruption (Coronal Mass Ejection - CME) on 29 May 2013 from SOHO Cameras

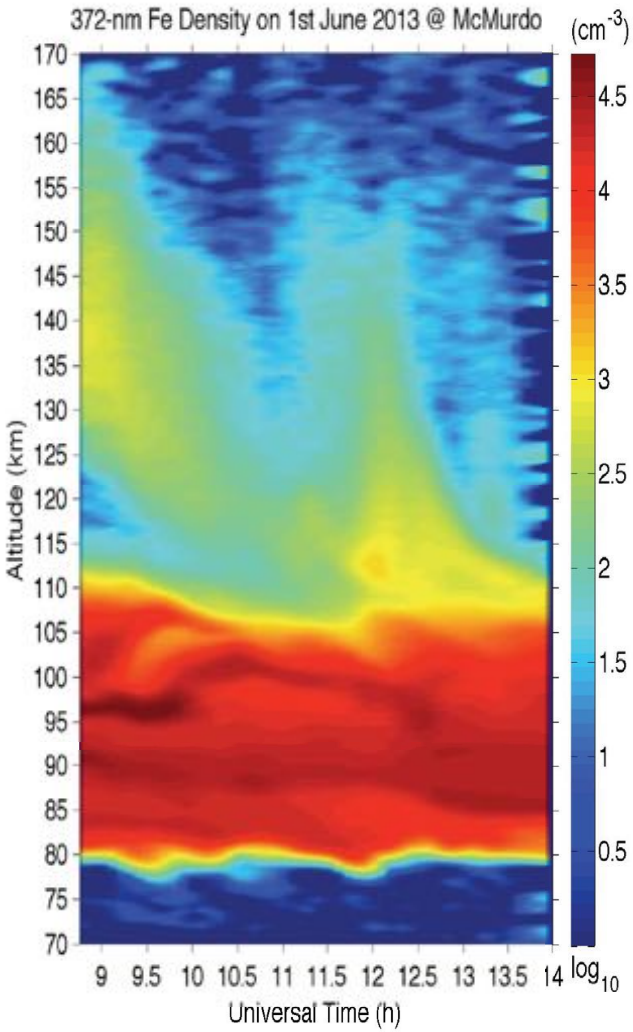

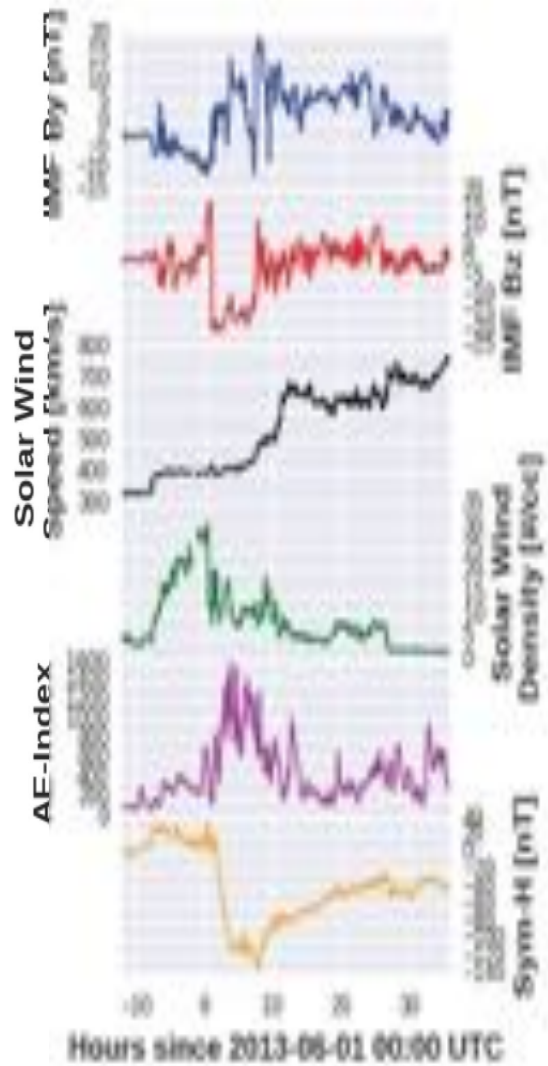

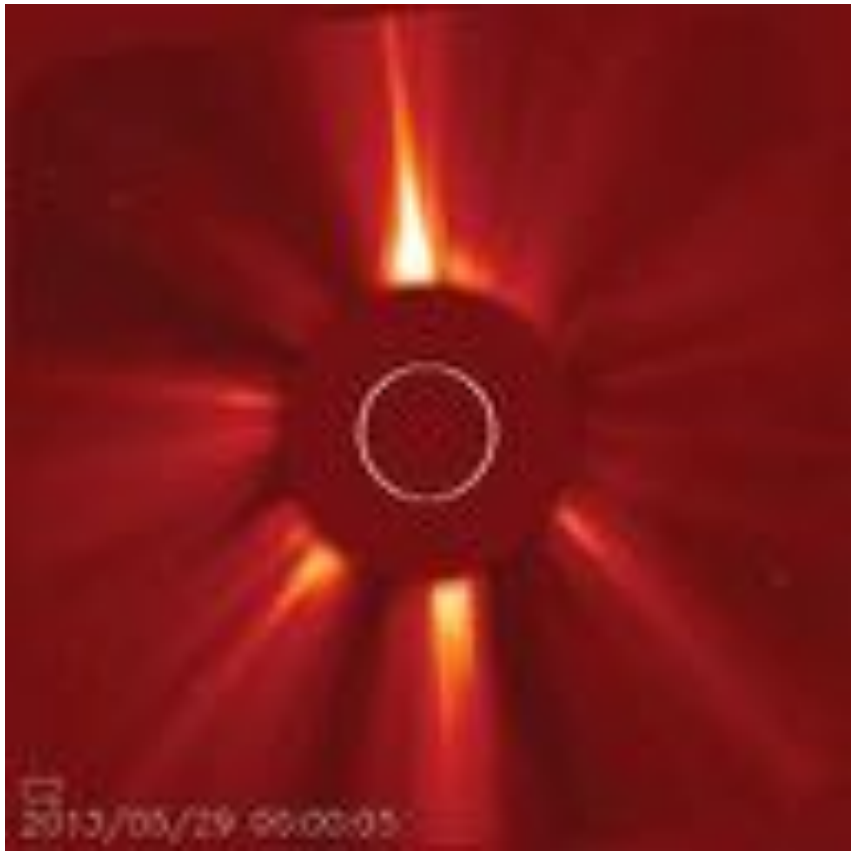

Courtesy of Dr. Delores Knipp

This CME on 29 May 2013 takes ~2 days to reach the Earth on 1 June 2013, followed by a High-Speed Stream (HSS).

"Predicting" TIFe Layers from Dst Magnetic Index

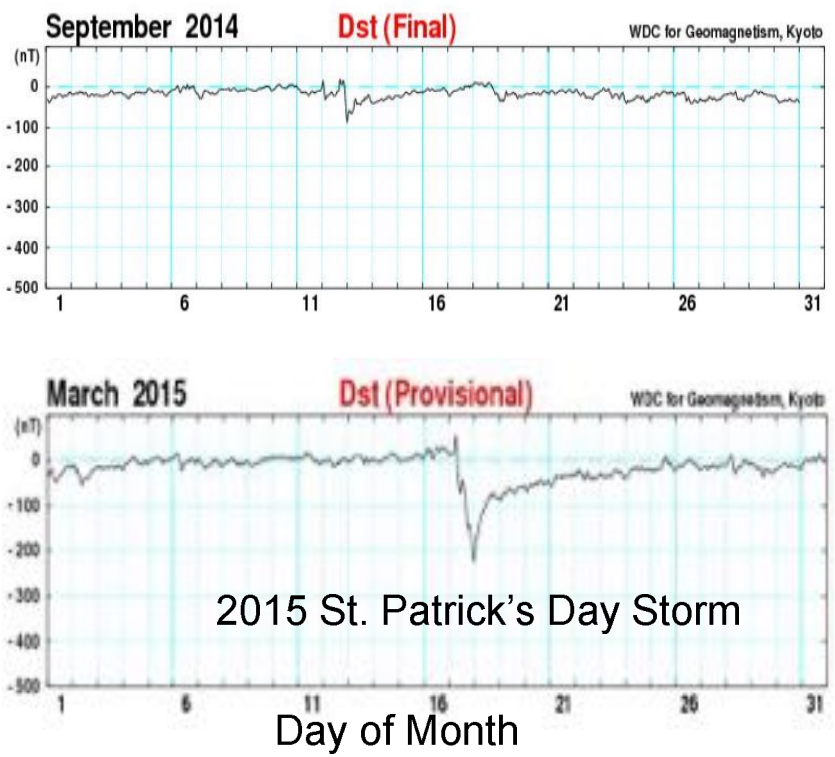

Fe Layers on 9/13/2014 and 3/16-17/2015 @ McMurdo

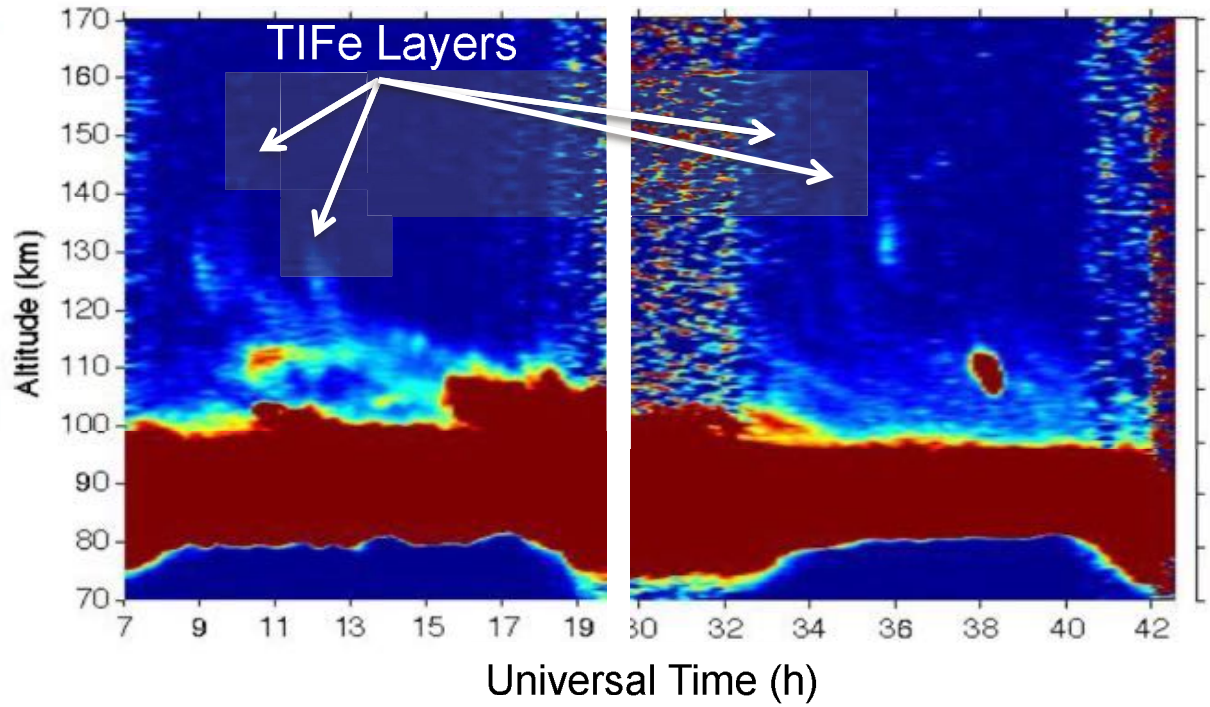

Fe Layers on 14-18 April 2016 @ McMurdo

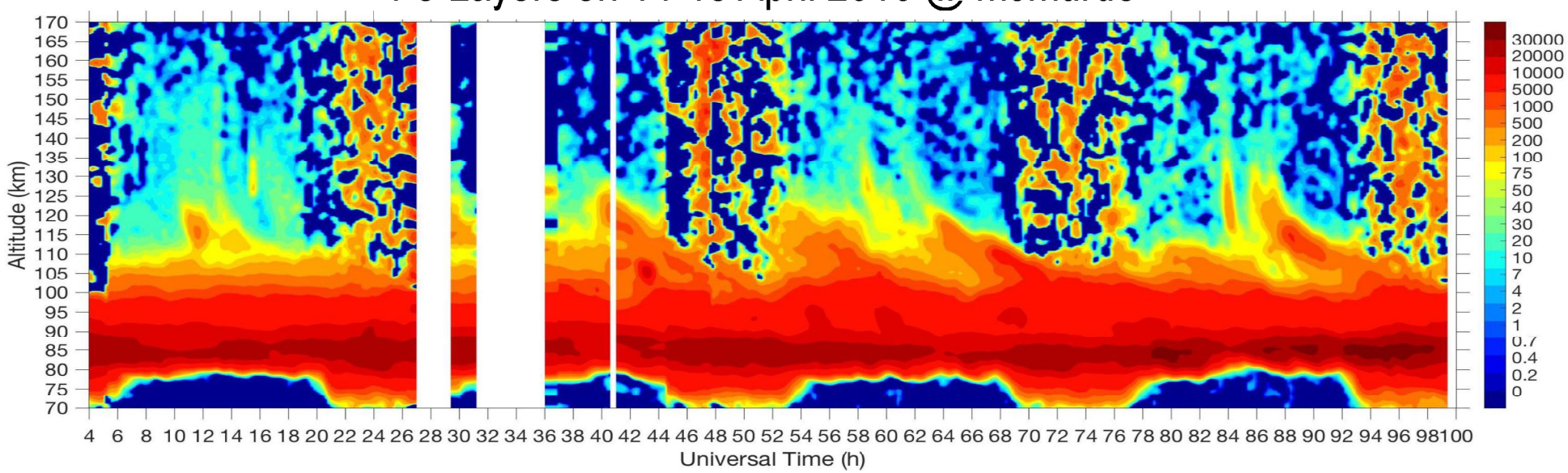

Horizontal Transport, Joule Heating, Substorms ...

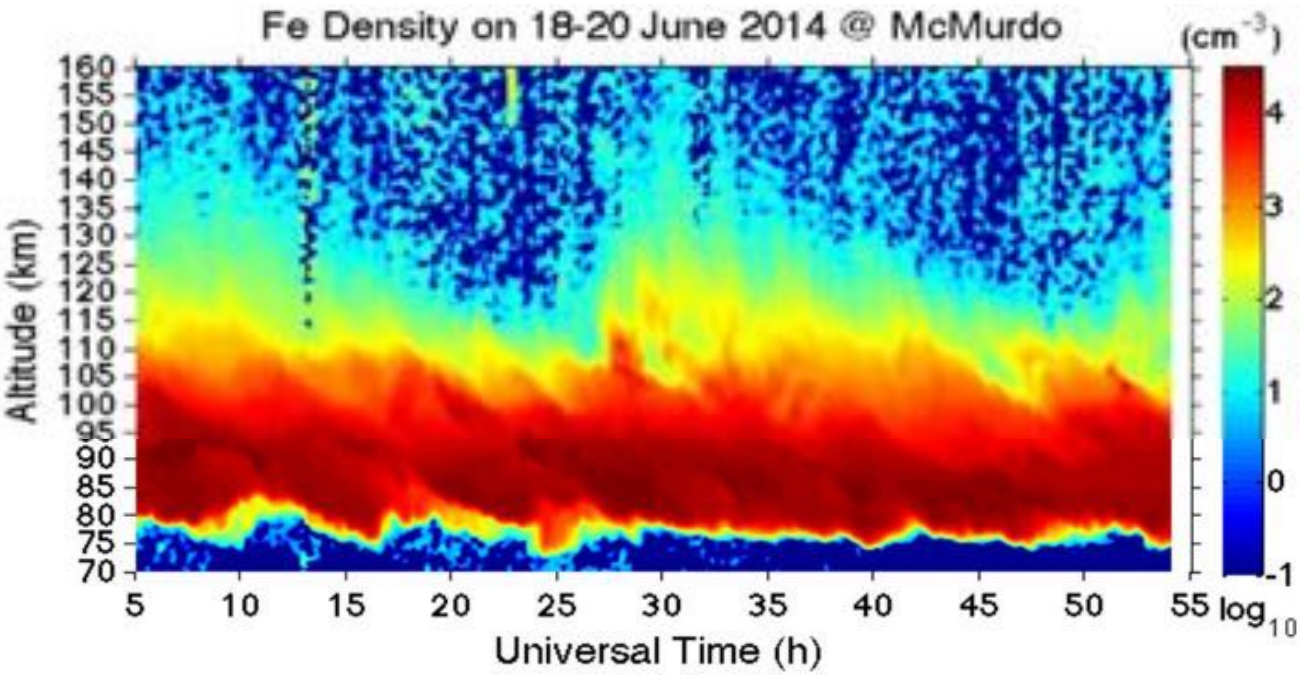

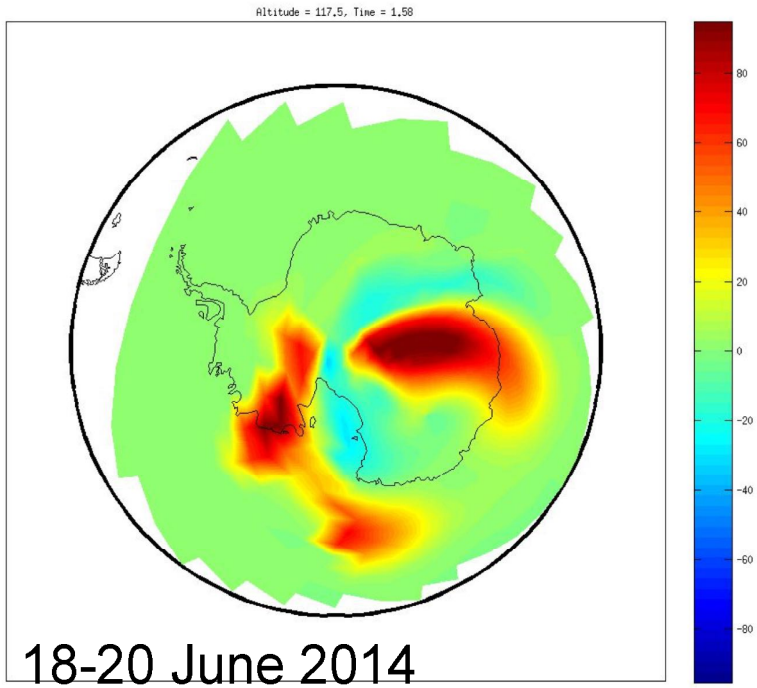

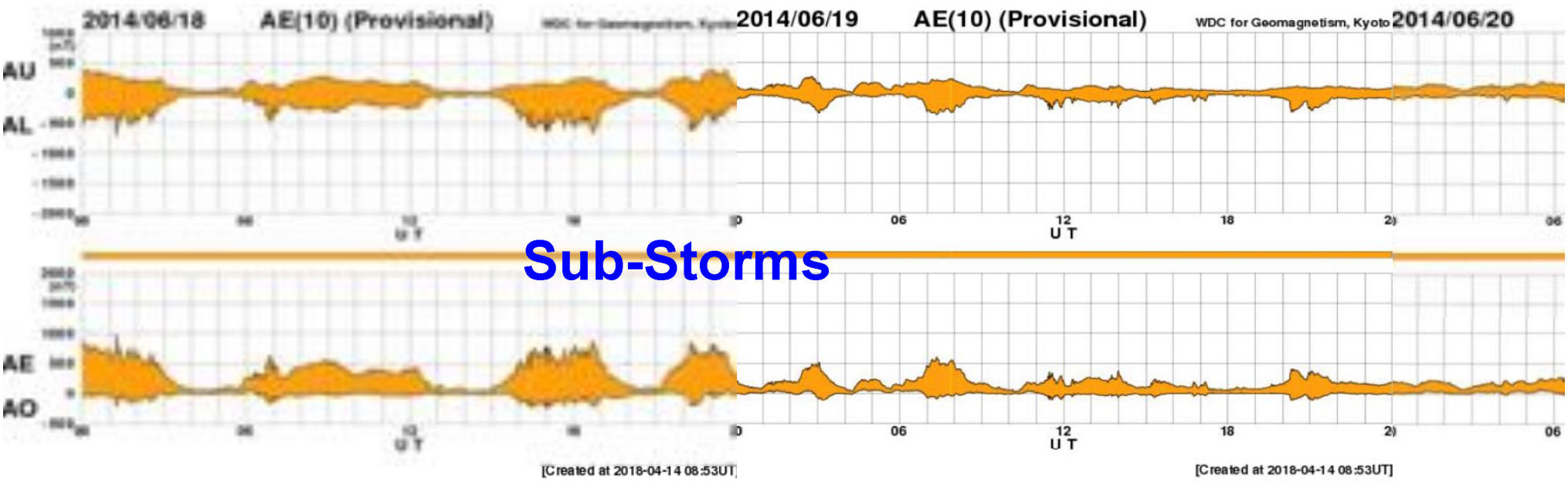

Sub-Storms

Conclusions and Future Work

What we have modeled so far is a major mechanism of TIFe layer formation, but it doesn't rule out other possibilities.

TIFe layer mechanisms can apply to other metals → TIMt

If Chu and Yu (2017) mechanism is the dominant process, then we expect TIMt layers occurring more frequently in the polar and tropical regions than at mid-latitudes, because of the available electric field (polar and fountain effects) – consistent with observations so far.

Particle precipitation and GLOW: driven with more realistic particle precipitation input (non-Maxwellian distribution)

Electric field: Weimer model updates, SuperDARN or other measurements, other models or new models

Besides geomagnetic storms, it is necessary to study the correlation between TIFe layers and sub-storms.

TIFe model to develop into a 3-D transport module interactive with GCMs

Conclusions and Outlook

1. The lidar-observed TIFe layers with the extraterrestrial origin open a new door to study the fundamental processes of AIM coupling and associated responses to solar and terrestrial inputs.
2. McMurdo lidar observations have enabled studies of wave coupling from bottom up, and investigation of M-I-T coupling from topside down. TIFe layers are a unique natural lab of space-atmosphere interaction.

More years of observations and model simulations are necessary to explore the TIMt layers and coupling to the AIM system & solar wind

Advancing Science Through Pushing Detection Limit

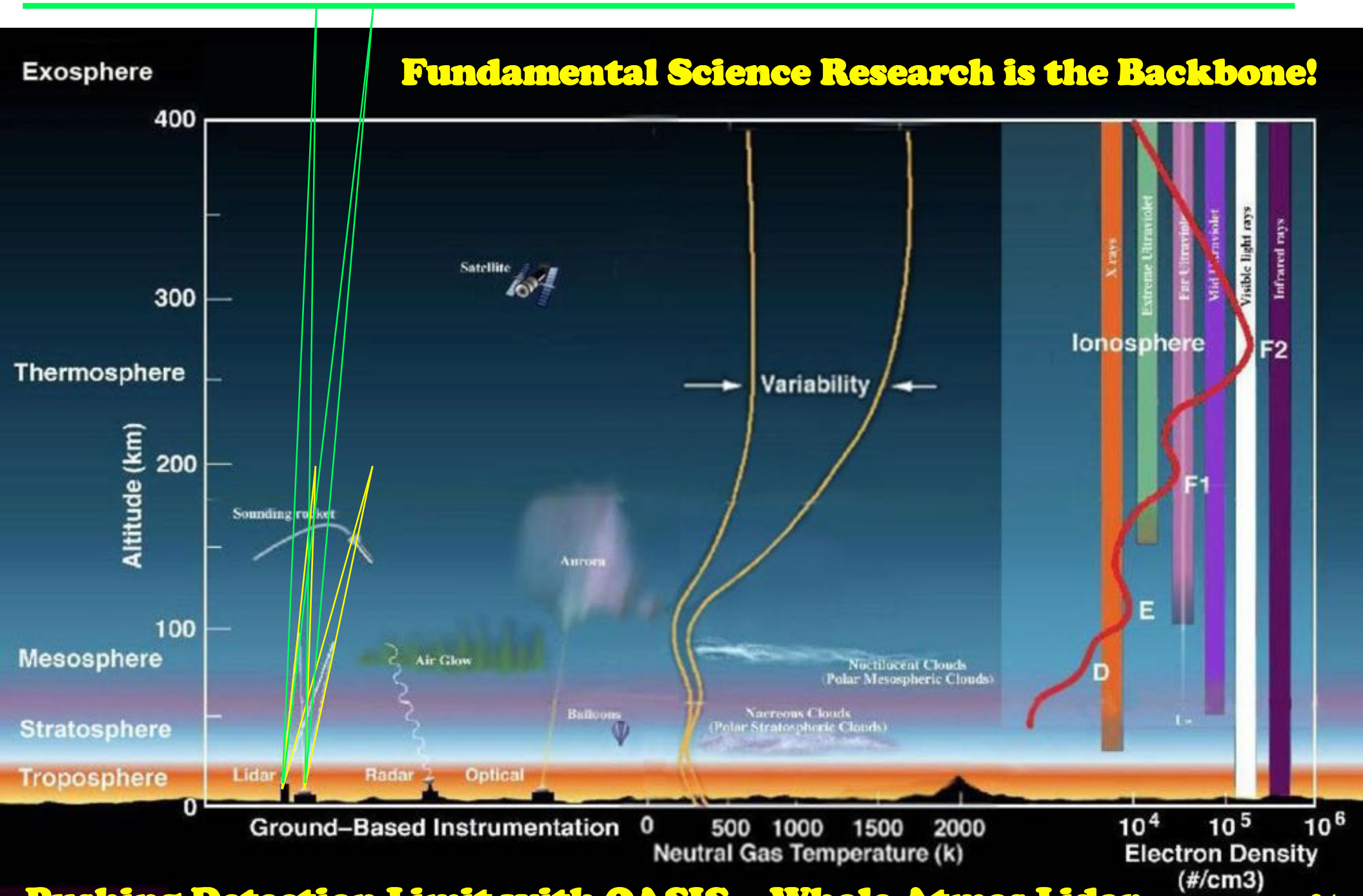

Advancing Science through Making Discoveries and Producing the Best Crop of Young Scientists

First Place Prizes at NSF/CEDAR student poster competitions

2011 Chihoko Yamashita
2012 Cao Chen
2013 Zhibin Yu
2015 Weichun Fong
2017 Ian Geraghty (undergrad)

Zhibin Yu	PhD	2014
John A. Smith	PhD	2014
Weichun Fong	PhD	2015
Cao Chen	PhD	2016
Brendan Roberts	MS	2012
Ian F. Barry	MS	2015